



RESEARCH ARTICLE

10.1029/2020MS002223

GFDL SHIELD: A Unified System for Weather-to-Seasonal Prediction

Key Points:

- A unified “one code, one executable, one workflow” global prediction modeling system is presented
- SHIELD’s multiple configurations show prediction skill and simulation fidelity matching or exceeding those of existing U.S. models
- The FV3 Dynamical Core provides a powerful foundation for unified prediction modeling

Supporting Information:

- Supporting Information S1

Correspondence to:

L. Harris,
lucas.harris@noaa.gov

Citation:

Harris, L., Zhou, L., Lin, S.-J., Chen, J.-H., Chen, X., Gao, K., et al. (2020). GFDL SHIELD: A unified system for weather-to-seasonal prediction. *Journal of Advances in Modeling Earth Systems*, 12, e2020MS002223. <https://doi.org/10.1029/2020MS002223>

Received 1 JUL 2020

Accepted 31 AUG 2020

Accepted article online 10 SEP 2020

Lucas Harris¹ , Linjiong Zhou^{1,2} , Shian-Jiann Lin¹, Jan-Huey Chen^{1,3} , Xi Chen^{1,2} , Kun Gao^{1,2} , Matthew Morin^{1,3} , Shannon Rees^{1,3}, Yongqiang Sun^{1,2} , Mingjing Tong^{1,4}, Baoqiang Xiang^{1,3} , Morris Bender^{1,2}, Rusty Benson¹ , Kai-Yuan Cheng^{1,2}, Spencer Clark^{1,5}, Oliver D. Elbert^{1,5}, Andrew Hazelton^{1,2,6}, J. Jacob Huff^{1,3}, Alex Kaltenbaugh^{1,3}, Zhi Liang¹ , Timothy Marchok¹, Hyeyum Hailey Shin^{1,3} , and William Stern¹

¹NOAA/Geophysical Fluid Dynamics Laboratory, Princeton, NJ, USA, ²Cooperative Institute for Modeling the Earth System, Program in Oceanic and Atmospheric Sciences, Princeton University, Princeton, NJ, USA, ³University Corporation for Atmospheric Research, Boulder, CO, USA, ⁴SAIC, Princeton, NJ, USA, ⁵Vulcan, Inc., Seattle, WA, USA, ⁶Now at NOAA/Atlantic Oceanographic and Meteorological Laboratory, Miami, FL, USA

Abstract We present the System for High-resolution prediction on Earth-to-Local Domains (SHIELD), an atmosphere model developed by the Geophysical Fluid Dynamics Laboratory (GFDL) coupling the nonhydrostatic FV3 Dynamical Core to a physics suite originally taken from the Global Forecast System. SHIELD is designed to demonstrate new capabilities within its components, explore new model applications, and to answer scientific questions through these new functionalities. A variety of configurations are presented, including short-to-medium-range and subseasonal-to-seasonal prediction, global-to-regional convective-scale hurricane and contiguous U.S. precipitation forecasts, and global cloud-resolving modeling. Advances within SHIELD can be seamlessly transitioned into other Unified Forecast System or FV3-based models, including operational implementations of the Unified Forecast System. Continued development of SHIELD has shown improvement upon existing models. The flagship 13-km SHIELD demonstrates steadily improved large-scale prediction skill and precipitation prediction skill. SHIELD and the coarser-resolution S-SHIELD demonstrate a superior diurnal cycle compared to existing climate models; the latter also demonstrates 28 days of useful prediction skill for the Madden-Julian Oscillation. The global-to-regional nested configurations T-SHIELD (tropical Atlantic) and C-SHIELD (contiguous United States) show significant improvement in hurricane structure from a new tracer advection scheme and promise for medium-range prediction of convective storms.

Plain Language Summary At many weather forecasting centers where computer weather models are run, different models are run for different applications. However, each separate model multiplies the effort needed to maintain and upgrade each model and makes it difficult to move improvements between models. We present a new “unified” weather modeling system, System for High-resolution prediction on Earth-to-Local Domains, able to be configured for a variety of applications. This system uses a powerful computer code, FV3, to compute the fluid motion of the atmosphere at any scale and also able to zoom in on areas of interest to better “see” severe storms or intense hurricanes. We show how we started from a quickly assembled model for testing FV3 and then gradually improved the representation of different atmospheric processes and expanded into new uses for the system, including short-range severe thunderstorm prediction, hurricane forecasting, and forecasts out to as long as 6 weeks. We address some of the challenges that we faced and discuss prospects for future model improvements. Since many of the parts of System for High-resolution prediction on Earth-to-Local Domains are used by models being developed by the National Weather Service for use by weather forecasters, the advances described here can be rapidly introduced into those models, eventually improving official forecasts.

1. Unified Modeling at GFDL

As computing power increases, global atmosphere models are now capable of regular simulation at resolutions that had been the sole domain of regional atmospheric models. The Integrated Forecast System (ECMWF, 2019a, 2019b) of the European Center for Medium-Range Weather Forecasting runs on a 9-km grid, and the Global Forecast System (GFS; Sela, 2010) of the U.S. National Centers for Environmental

©2020. The Authors.

This is an open access article under the terms of the Creative Commons Attribution License, which permits use, distribution and reproduction in any medium, provided the original work is properly cited.

Prediction (NCEP) runs on a 13-km grid. Some CMIP-class (Coupled Model Intercomparison Project) climate models now use grids with spacings as fine as 25 km (Chen & Lin, 2013; Haarsma et al., 2017; Vecchi et al., 2019). Global atmosphere models lack the lateral boundary errors that contaminate the solutions of regional models after a few days of simulation. They thus allow us to extend mesoscale and storm-scale predictions into the medium range and beyond (Harris & Lin, 2013; Harris et al., 2014, 2019; Zhou et al., 2019). Global modeling also brings many new challenges—one cannot “throw your garbage in the neighbor’s yard” in global modeling, so to speak. Biases and radiative imbalances must be minimized, as must errors *anywhere* in the atmosphere that could potentially grow and contaminate the entire domain.

A unified modeling system supports a variety of applications at a wide range of spatial and temporal scales within a single framework. These systems promise to simplify operational and research modeling suites and better exchange improvements and bug fixes between applications. The Unified Model of the U.K. Met Office (Brown et al., 2012) is the most notable unified system. Variable-resolution models (Harris & Lin, 2014; McGregor, 2015) are particularly well suited for unified modeling as they can efficiently reach very high resolutions over part of the earth, replacing the highest-resolution regional models (Hazelton, Bender, et al., 2018; Hazelton, Harris, & Lin, 2018; Zhou et al., 2019) and potentially extending their lead times.

Here at the Geophysical Fluid Dynamics Laboratory (GFDL), a hierarchy of models has been developed for a variety of time and space scales, from centennial-scale earth-system simulations (Dunne et al., 2020) to very high-resolution weather prediction. The GFDL suite is unified around a single dynamical core, the GFDL Finite-Volume Cubed-Sphere (FV3) Dynamical Core (Putman & Lin, 2007), and a single framework, the Flexible Modeling System (Balaji, 2012), and other shared components. We describe one part of this suite, the System for High-resolution prediction on Earth-to-Local Domains (SHIELD). This model, previously called fvGFS, was developed as a prototype of the Next-Generation Global Prediction System of the National Weather Service and of the broader Unified Forecast System (UFS). SHIELD continues GFDL’s high-resolution global modeling program previously established using the High-Resolution Atmosphere Model (HiRAM; Chen & Lin, 2013; Zhao et al., 2009). SHIELD couples the nonhydrostatic FV3 dynamical core (Lin et al., 2017) to a physics suite originally from the GFS (Han et al., 2017, and references therein) and the Noah Land Surface Model (Ek et al., 2003). SHIELD can be used for a variety of time scales but has been designed with a particular focus on short-to-medium range weather (18 hr to 10 days) and into the subseasonal-to-seasonal (S2S; several weeks to several months) range. Seasonal-to-decadal predictions and centennial-scale climate projections coupled to a dynamical ocean are performed at GFDL using the Seamless System for Prediction and Earth System Research (Delworth et al., 2020), the Coupled Model Version 4 (CM4; Held et al., 2019), and the Earth System Model Version 4 (Dunne et al., 2020).

Since FV3 is designed to adapt to a variety of purposes and to any scale of atmospheric motion, it is an ideal platform for a unified modeling system. All of the SHIELD configurations described here, as well as regional and doubly periodic applications lying beyond the scope of this paper, use the same code base, the same executable, the same preprocessor, the same runscripts, and same postprocessing tools, demonstrating a true unification for modeling on weather-to-S2S time scales. This approach also suggests how further unification with GFDL’s climate models may proceed, which use a different atmospheric physics (Zhao et al., 2018), the MOM6 Dynamical Ocean (Modular Ocean Model, version 6; Adcroft et al., 2019), and the GFDL Land Model, version 4 (LM4) land model. Advances in SHIELD can be seamlessly moved into other UFS models, including the 2019 upgraded GFSv15, and other FV3-based models. Most notably, advances in SHIELD can migrate into UFS models slated for operational implementation at NCEP, including the FV3-based GFSv15. NASA GEOS (National Aeronautics and Space Administration Goddard Earth Observing System; Putman & Suárez, 2011), NASA/Harvard GEOS-Chem High-Performance, The Community Earth System Model version using the FV3 dynamical core, and the Chinese Academy of Sciences’ FGOALS (Flexible Global Ocean-Atmosphere-Land System Model; Guo et al., 2020) all also use FV3 as their dynamical core and can benefit from the advances described below. This diversity of FV3-based models shows the advantages of using common components to leverage advances in the dynamical core but while still allowing centers to tailor their models to their own needs, the freedom to innovate new model designs, and to encourage the development of models as holistic-integrated systems, rather than clumsily joining independent components.

SHIELD is designed for exploratory research into model design and development, with a focus on dynamics and physics-dynamics integration, and for research on prediction and atmospheric processes on time scales

from a few hours to a few months. SHIELD is currently focused on deterministic prediction although effective S2S prediction will require the development of a simple ensemble (cf. Chen & Lin, 2013). In this manuscript we use forecast skill as a principal means of establishing the scientific credibility of SHIELD as a research tool. Further research will more closely evaluate specific structures and processes within SHIELD, with some initial results described below (especially section 3.2) and in prior research (cf. Hazelton, Bender, et al., 2018).

The design, evolution, configurations, and simulation characteristics of SHIELD are the subject of this paper. Section 2 describes the components of SHIELD and how they work together as a complete modeling system. Section 3 describes the four configurations of SHIELD for a variety of applications, including medium-range weather, continental convection, tropical meteorology and hurricanes, and S2S prediction. Section 4 summarizes the history of SHIELD development and discusses prospects for future work.

2. SHIELD Components

2.1. Nonhydrostatic FV3 Dynamical Core

All SHIELD simulations use the nonhydrostatic solver within the FV3 Dynamical Core. This core has been described in detail in other papers (Harris & Lin, 2013; Lin, 2004; Putman & Lin, 2007, and references therein) and will only be summarized here. FV3 solves the fully compressible Euler equations on the gnomonic cubed-sphere grid and a Lagrangian vertical coordinate. Fast vertically propagating sound and gravity waves are solved by the semi-implicit method; otherwise, the algorithm is fully explicit. FV3 advances sound and gravity wave processes and advects thermodynamic variables on the shortest “acoustic” timestep, while subcycled tracer advection and vertical remapping (cf. Lin, 2004) are performed on an intermediate “remapping” timestep, in turn performed multiple times per physics timestep.

FV3’s discretization along Lagrangian surfaces uses the piecewise-parabolic method, which previously used a monotonicity constraint to ensure positivity and to dissipate energy cascading to grid scale. In nonhydrostatic FV3, dynamical quantities (vorticity, potential temperature, and air mass) are advected by a nonmonotonic scheme to reduce dissipation of resolved-scale modes. Previous work with nonhydrostatic FV3 had continued to use a monotonic advection scheme to avoid unphysical negative values. In this manuscript we present results using a new *positive-definite* (PD) but nonmonotonic scheme to advect tracers, which greatly improves the representation of marginally resolved and discontinuous features without creating computational noise at sharp gradients. This scheme is described in detail in Appendix A and applications to the representation of tropical cyclones in section 3.2.

2.2. GFS/SHIELD Physics and Noah LSM

SHIELD inherits the GFS suite of physical parameterizations developed by the Environmental Modeling Center of NCEP (2020). The initial 2016 version of SHIELD, implemented for dynamical core testing during Phase II of Next-Generation Global Prediction System, used physics largely identical to the then-operational GFSv13: the Simplified Arakawa-Schubert (SAS) shallow and deep convection schemes described in Han and Pan (2011); the hybrid eddy-diffusivity mass-flux (EDMF) scheme (Han et al., 2016); the Rapid Radiative Transfer Model (Clough et al., 2005); the microphysics of Zhao and Carr (1997) and cloud-fraction scheme of Xu and Randall (1996); the Navy’s simplified ozone scheme (McCormack et al., 2006); the GFS orographic gravity wave drag and mountain blocking schemes (Alpert, 2004); and the convective gravity wave drag scheme of Chun and Baik (1998).

We have since made many changes to the physics to be able to support new applications, especially for convective-scale prediction and marine phenomena, or to take advantage of new capabilities within the FV3 dynamical core. We first introduced the six-category GFDL microphysics and cloud fraction scheme (Zhou et al., 2019) with the fast microphysical processes split out of the physics driver and taking place on the shorter remapping timestep. Later, the GFDL microphysics was fully in-lined within FV3 (Appendix B). Several new planetary boundary layer (PBL) schemes have also been used in SHIELD, including a modified hybrid eddy-diffusivity mass-flux (EDMF) PBL as per Zhang et al. (2015), and the Yonsei University scheme (YSU; Hong, 2010, Hong et al., 2006, Wilson & Fovell, 2018). We have also adopted the Scale-Aware SAS (Han et al., 2017) convection scheme in more recent versions of SHIELD.

The land surface model is the Noah Land Surface Model (Ek et al., 2003), integrated within the physics and paired to the GFS surface-layer scheme. In 2017, Noah was upgraded to use the high-resolution land surface data (Wei et al., 2017), which greatly improves the appearance of land-surface fields in convective-scale simulations.

2.3. MLO

Initially, sea surface temperatures (SSTs) were prescribed as the climatological SST plus an SST anomaly from initial conditions which gradually decays to zero, without influence from the atmosphere. However, air-sea interactions are critical for several phenomena of interest to us, especially tropical cyclones and the Madden-Julian Oscillation (MJO), and may impact large-scale skill as well. To incorporate atmosphere-ocean interaction, we have implemented a modification of the mixed layer ocean (MLO) of Pollard et al. (1973). This simple ocean computes the mixed layer depth and heat within that mixed layer as prognostic variables, with tendencies computed from the net surface heat flux. The SST is nudged toward the NCEP Real-Time Global SST (Thiébaux et al., 2003) climatology plus a fixed initial anomaly which decays with a fixed time scale. The ocean mixed layer depth is also nudged toward observed climatology (de Boyer Montégut et al., 2004). While considerably simpler than the three-dimensional dynamical oceans in CM4 (Held et al. 2019) and in the GFDL Hurricane Model (Bender et al., 2019), the MLO still represents the thermodynamic and dynamic ocean interactions of greatest significance on the time scales for which SHIELD is used (Hazelton, Harris, & Lin, 2018), without incurring the complexity of a three-dimensional dynamical ocean.

2.4. Interoperability With Other UFS Models

SHIELD was designed to work with other models that use FV3, Flexible Modeling System, the GFS Physics Driver, and/or the Interoperable Physics Driver (IPD). The IPD is the interface between FV3 and the GFS Physics Driver, although it can support other physics suites. Innovations within SHIELD can then be seamlessly exchanged with other models using these same components. The UFS Atmosphere led by NCEP (<https://github.com/NOAA-EMC/fv3atm/>) is analogous to SHIELD. For example, the transition of FV3 and the GFDL Microphysics into the operational GFSv15 was accelerated by the IPD. Conversely, schemes which have been introduced into the GFS Physics Driver by the broader community can then be integrated into SHIELD, including the numerous schemes implemented by Zhang et al. (2019).

3. SHIELD Configurations

SHIELD leverages the flexibility of FV3 to be able to make accurate and efficient simulations at a variety of spatial and temporal scales. Much of the development of SHIELD (and previously, of HiRAM) has been driven by a desire to improve the simulation quality at the convection-permitting resolutions covered by the range of SHIELD configurations.

We present four different configurations of SHIELD. All configurations are global domains using either a uniform grid or a locally refined grid using nesting or stretching (Harris & Lin, 2013; Harris et al., 2016; Zhou et al., 2019). SHIELD can also run on FV3's doubly periodic domain (Arnold & Putman, 2018; Held et al., 2007) or on a regional domain using any regular quadrilateral grid (Dong et al., 2020), at spatial resolutions down to a few tens of meters (Jeevanjee, 2017). These applications lie beyond the scope of this paper.

The four configurations can be fit within two “tiers”; Tier-1 configurations are the most well tested, having originally been developed as prototypes to replace legacy NCEP models by FV3-based UFS systems and having been run in near-real time for several years. These configurations demonstrate the capabilities of SHIELD, allow direct comparison to existing operational models, and provide robust tests of the forecast skill and reliability of SHIELD. Current real-time configurations are run twice daily and displayed online (<https://shield.gfdl.noaa.gov/>).

The Tier-1 configurations are our flagship 13-km SHIELD, a prototype for the now-operational GFSv15 and for future upgrades of the GFS; (Tropical) T-SHIELD with a static, 3-km nest spanning the tropical North Atlantic, a prototype of the Hurricane Analysis and Forecast System (HAFS); and (Continental) C-SHIELD with a 3-km nest over the contiguous United States (CONUS), a prototype of the Regional Forecast System (RFS). Each of the Tier-1 configurations are usually refreshed every year with a new version, indicated by the year of the upgrade.

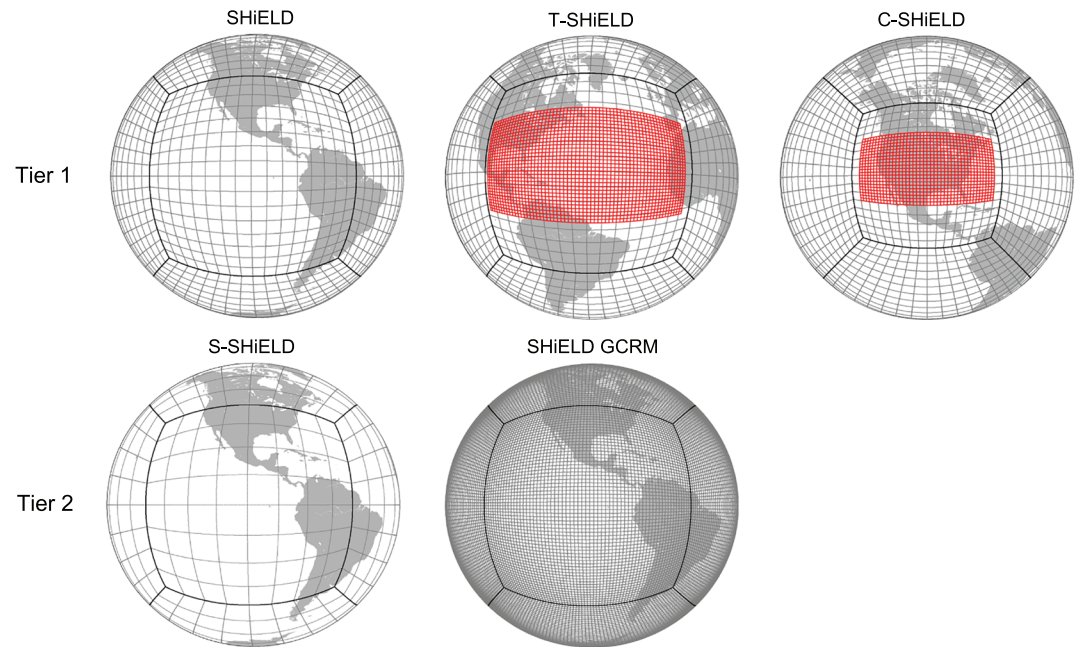


Figure 1. Current SHiELD configurations. Each plotted cell is 48×48 actual grid cells. Heavy black lines represent cubed-sphere edges; red lines represent nested grids. Note that the global domain of C-SHiELD (top center) is slightly stretched as per Harris et al. (2019).

Our Tier-2 configurations address new challenges for numerical prediction and are still under development. Our 25-km (Subseasonal) S-SHiELD addresses the challenging domain of S2S prediction. Another configuration not discussed in this paper is the SHiELD global cloud-resolving model and addresses the frontier computational and data challenges of such simulations. This configuration was submitted to the DYnamics of the Atmospheric general circulation Modeled On Nonhydrostatic Domains intercomparison (Sato et al., 2019; Stevens et al., 2019). Both configurations inspire the development of new functionality and capabilities within SHiELD and readily expose instabilities, climate drift, conservation issues, and other shortcomings. The advances driven by work on these frontier challenges help improve the Tier-1 configurations, demonstrating the value of a seamless prediction system. The domains for each of the four configurations plus the global cloud-resolving model configuration are depicted schematically in Figure 1.

Although all configurations follow the unified “one code, one executable, one workflow” structure of SHiELD, the configurations are not identical owing to the need to tailor each configuration for its specific application. Further, given the rapid pace of SHiELD development and the staggered development cycle for some of the configurations, we do not expect all of the Tier-1 configurations to always have the very latest developments. The development paths of the different SHiELD configurations can be seen in Table 1.

All configurations are initialized using the real-time GFS analyses made available by NCEP following Chen et al. (2018). This “cold starting” from the hydrostatic, spectral GFS could potentially leave the convective-scale configurations (T-SHiELD and C-SHiELD) at a comparative disadvantage to models with native, specialized convective-scale data assimilation. This issue is minimized here due to the ability of FV3-based models to “spin up” their convective scales within a few hours of initialization and experience little degradation thereafter (Harris et al., 2019; Hazelton, Bender, et al., 2018; Hazelton, Harris, & Lin, 2018; Marchok et al., 2018; Zhang et al., 2019).

Computational efficiency is crucial for useful simulation modeling, for both real-time and experimental applications. We present the timings for the most recent iterations of SHiELD in Table 2. The 13-km SHiELD needs only 3,096 processor cores to complete 1 day in under 8.5 min, the threshold traditionally used for operational global prediction. The 25-km S-SHiELD completes 1.5 years per day with just over 1,700 cores; we are hoping to improve the computational cost as part of further S-SHiELD development. C-SHiELD is necessarily more expensive owing to its nested grid but still completes a 5-day simulation in

Table 1
Development of the Four SHIELD Configurations and Their Yearly Revisions Described in This Paper

Configuration	SHIELD				T-SHIELD				C-SHIELD				S-SHIELD		
	2016	2017	2018	2019	2017	2018	2017	2018	2017	2018	2017	2018	2019	2019	2019
Version	2015/01– 2016/12	2015/01– 2016/12	2016/01– 2017/12	2017/01– 2018/12	2017/08/18– 2017/10/06	2017/08/18– 2017/10/06	2017/05– 2018/04	2018/05– 2019/03	2019/04– 2019/12	2019/04– 2019/12	2019/04– 2019/12	2019/04– 2019/12	2019/04– 2019/12	2019/04– 2019/12	2019/04– 2019/12
Simulation frequency	00Z every 5 days	00Z every 5 days	00Z every 5 days (hindcast)	00Z every 5 days (hindcast)	4× daily	4× daily	20-to-9 km stretched (c768r15) + 3-km 3× nest (2,016 × 1,080)	00Z daily	00Z every 2 days	00Z every 2 days					
Simulation length	10 days	10 days	10 days	10 days	126 hr	126 hr	20-to-9 km stretched (c768r15) + 3-km 3× nest (2,016 × 1,080)	120 hr	40 days	40 days					
Resolution	13 km (c768)	13 km (c768)	13 km (c768)	13 km (c768)	13 km (c768) + 3-km nest (2,880 × 1,536)	13 km (c768) + 3-km nest (2,880 × 1,536)	20-to-9 km stretched (c768r15) + 3-km 3× nest (2,016 × 1,080)	25 km	25 km						
Grid cells	3.54 M	3.54 M	3.54 M	3.54 M	3.54 M + 4.23 M	3.54 M + 4.23 M	3.54 M + 2.18 M	3.54 M + 2.18 M	3.54 M + 2.18 M	3.54 M + 2.18 M	3.54 M + 2.18 M	3.54 M + 2.18 M	3.54 M + 2.18 M	885 K	885 K
Vertical levels	63	63	91	91	63	63	63	63	63	63	63	63	63	91	91
Physics timestep	225	150	150	150	90	90	90	90	90	90	90	90	90	450	450
Remapping, tracer, and MP timestep	112.5	150	150	150	90/22.5	90/22.5	90/22.5	90/22.5	90/22.5	90/22.5	90/22.5	90/22.5	90/22.5	225	225
Acoustic timestep	18.75	18.75	18.75	18.75	12.8/4.5	12.8/4.5	12.8/4.5	12.8/4.5	12.8/4.5	12.8/4.5	12.8/4.5	12.8/4.5	12.8/4.5	28.125	28.125
Tracer advection scheme	Monotonic	Monotonic	Pos. def	Pos. def	Monotonic	Monotonic	Monotonic	Pos. def	Pos. def	Monotonic	Monotonic	Pos. def	Pos. def	Pos. def	Pos. def
Microphysics PBL scheme	Zhao-Carr Hybrid EDMF	Split GFDL Hybrid EDMF	Inline GFDL YSU	Inline GFDL YSU	Split GFDL Mod. EDMF	Split GFDL Mod. EDMF	Split GFDL Mod. EDMF	Split GFDL YSU	Split GFDL YSU	Split GFDL Mod. EDMF	Split GFDL Mod. EDMF	Split GFDL YSU	Split GFDL YSU	Inline GFDL YSU	Inline GFDL YSU
Deep convection scheme	SAS	SA-SAS	SA-SAS	SA-SAS	SAS	SAS	None	SA-SAS	SA-SAS	None	None	None	None	SAS	SAS
Ocean surface	Specified	Specified	MLO	MLO	Specified	Specified	Specified	MLO	MLO	Specified	Specified	Specified	MLO	MLO	MLO

Note. Timesteps are given in seconds; for nested simulations, the format is global/nested timesteps. All configurations and versions use the same Noah LSM and RRTM, and all use SAS or SA-SAS shallow convection except 2017 and 2018 C-SHIELD.

Table 2
Performance and Computational Load of SHiELD Configurations

	#Grid columns	Vertical levels	Processor cores	Time/1 day (min)	Core hours per simulated day	Cost relative to SHiELD
S-SHiELD 2019	885 K	91	1,728	2.5	72.0	0.18
SHiELD 2019	3.54 M	91	3,072	7.7	394.2	1.
T-SHiELD 2018	3.54 M + 4.23 M	63	3,168	33.4	1,763.5	4.47
C-SHiELD 2019	3.54 M + 2.18 M	63	3,420	23.4	1,333.8	3.38

Note. Average performance statistics over a number of simulations are given. Time per day includes the initialization, termination, and I/O. All simulations were done on the C4 partition of Gaea, a Cray XC40 supercomputer with Intel Broadwell processors. All SHiELD simulations use FV3's nonhydrostatic solver.

under 2 hr on less than 3,500 cores. T-SHiELD has a nested grid with twice as many columns as C-SHiELD but is only about 30% more expensive.

SHiELD is compiled with mixed-precision arithmetic: The dynamics (and the inlined components of the microphysics) use single-precision arithmetic, while the physics uses double precision. This differs from the practice used for most operational models (GFSv15 excluded) and for GFDL climate models, which use double-precision arithmetic throughout. Tests with the 2016 version of SHiELD had found no detectable difference in skill between predictions using mixed-precision and double-precision arithmetic while leading to a cost reduction of about 40%.

3.1. SHiELD Medium-Range Weather Prediction

The flagship SHiELD configuration is designed for medium-range prediction with lead times of 24 hr to 10 days. The design of SHiELD is similar to the operational GFS: a global c768 grid—a cubed-sphere with each face having 768×768 grid cells—with an average grid-cell width of about 13 km. The 2016 and 2017 versions of SHiELD used 63 vertical levels (Figure 2), the same as the hydrostatic GFSv14 but with the uppermost semi-infinite layer removed to permit nonhydrostatic simulation. SHiELD 2017 was then developed by NCEP and partners to become GFSv15 and its GFS Data Assimilation System: Specific implementation details can be seen online (https://www.emc.ncep.noaa.gov/emc/pages/numerical_forecast_systems/gfs/implementations.php). Starting in 2018, SHiELD increased the number of vertical levels to 91, increasing the number of vertical levels below 700 mb from 19 to 23 and decreasing the depth of the lowest model layer from 45 to 33 m.

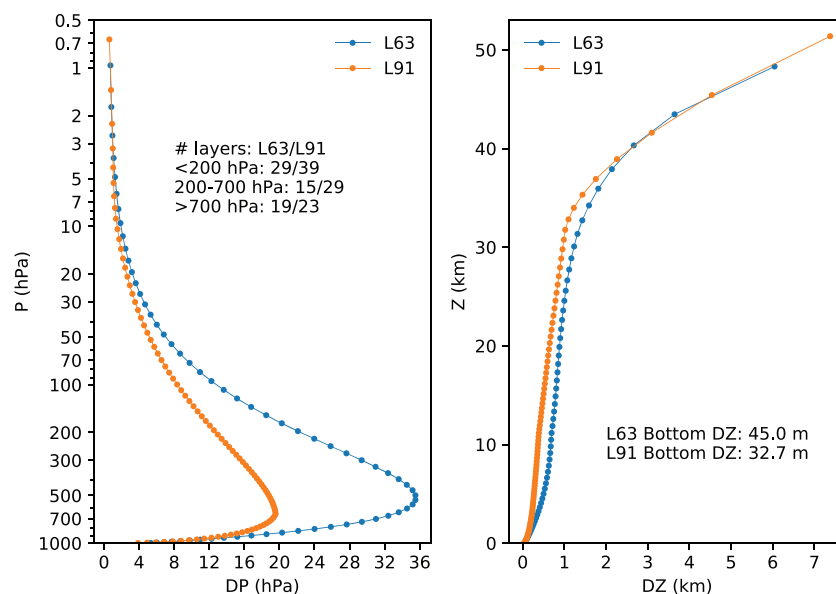


Figure 2. Distribution of vertical levels in various SHiELD configurations for a surface pressure of 1,000 hPa and a standard atmospheric temperature structure.

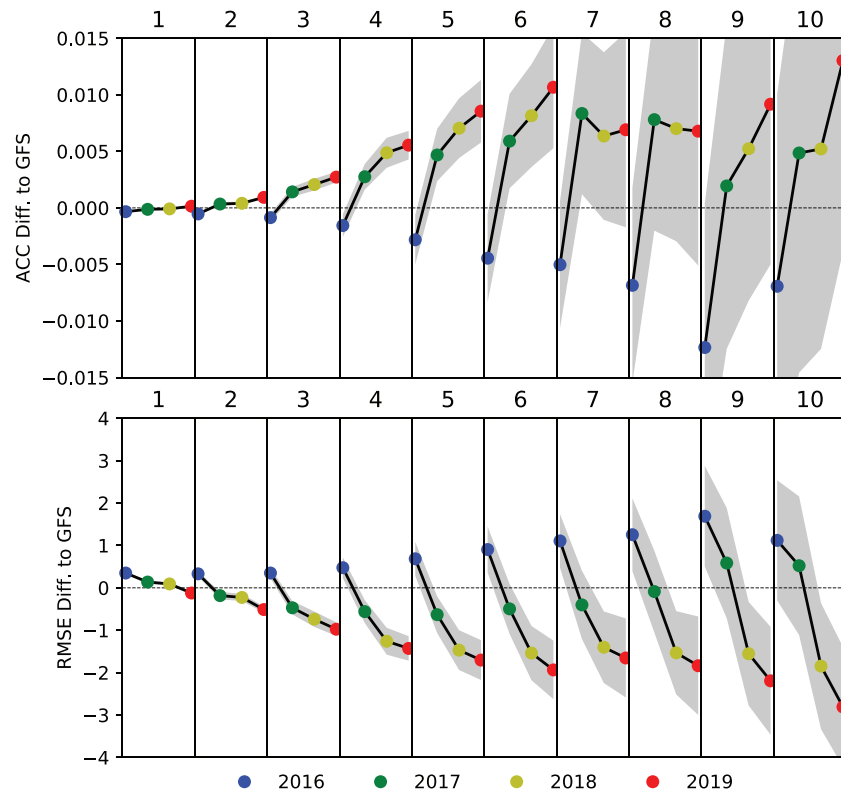


Figure 3. Global 500-mb geopotential height ACC (top) and RMSE (bottom, m) difference from the contemporary GFS as a function of lead time (instantaneous at 00Z each day after initialization) for each version of the 13-km SHiELD. Gray shading is the 95% confidence interval. Each version of SHiELD is evaluated with 2 years of 10-day hindcasts initialized at 00Z every 5 days, for a total of 144 cases per version. See Table 1 for the time periods being compared here.

The simulation characteristics and prediction skill of SHiELD have been previously discussed in several papers and will not be repeated here. Improving predictions of tropical cyclone track, intensity, and genesis has been a key driver of SHiELD development: Chen, Lin, Magnusson, et al. (2019) describes the 2016 and 2017 versions, while the considerably improved 2018 version is described in Chen, Lin, Zhou, et al. (2019). Most notably SHiELD greatly improves upon other global models' ability to predict tropical cyclone intensity. The large-scale prediction skill and CONUS precipitation and 2-m temperature skill are briefly described for the 2016 and 2017 versions in Zhou et al. (2019) and Harris et al. (2019).

The anomaly correlation coefficient (ACC) of the 500-mb geopotential height field is the standard means for evaluating the large-scale prediction skill of medium-range prediction models. Figure 3 (top) shows that the global ACC of SHiELD has been better at all lead times than the contemporary GFS since the 2017 version and significantly so on Days 1–6. At all lead times except for Days 7 and 8, each new version has improved upon the previous version. The result for root-mean square error (RMSE; Figure 3, bottom) is even more striking: Every version is an improvement upon the previous at every lead time, and both the 2018 and 2019 versions are significantly better than the operational GFS. Results for just the Northern Hemisphere (20–80°N; supporting information Figure S1) are less dramatic, but SHiELD still shows statistically significant improvements in ACC and RMSE out to Day 5. Both the GFS and all versions of SHiELD reach an ACC of 0.6 at 8.3–8.5 days globally and 8.5–8.7 days in the Northern Hemisphere, with some year-to-year and version-to-version variabilities.

The time series of Day 5 global ACC and RMSE (Figure 4) shows that while there is a general secular improvement in both SHiELD and the GFS, there can be large seasonal and even interannual variability in forecast skill. Usually, predictions are more skillful in northern winter, as strong synoptic forcing dominates the large-scale weather patterns, but some northern summers see little to no forecast degradation. The implementation of GFSv13 on 11 May 2016, which included a major upgrade to the data assimilation

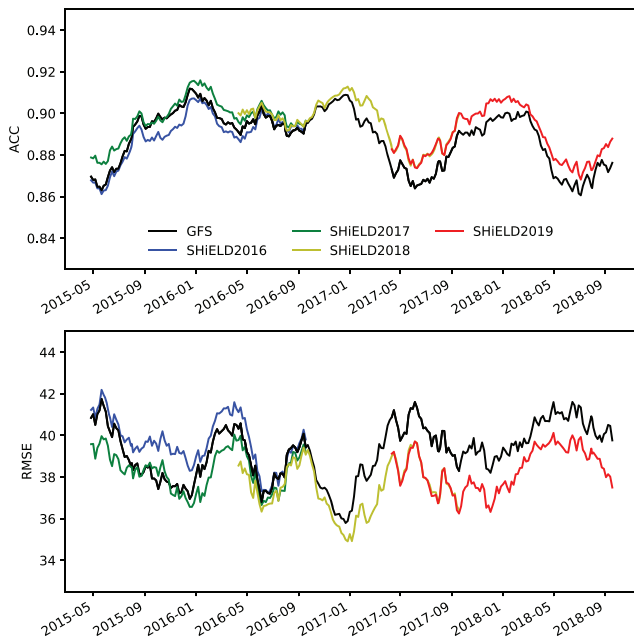


Figure 4. Six-month running-mean time series of global 500-mb geopotential height ACC (top) and RMSE (bottom, m) at Day 5 for each version of the 13-km SHiELD and the contemporary operational GFS. Note that the operational GFS upgraded to v13 on 11 May 2016 and v14 on 19 July 2017.

cycling system of the GFS, significantly reduced RMSE in May and June 2016 compared to the preceding four months of the year. These results are worthy of further investigation. We do conclude that it may be misleading to use a short time period to evaluate or compare global prediction models.

The time evolution of the large-scale forecast skill for both the GFS and SHiELD are very similar on monthly and shorter time periods, which is expected as they use identical initial conditions, and SHiELD benefits from continual upgrades of the GFS initial conditions. As discussed in Chen, Lin, Zhou, et al. (2019), the quality of the initial conditions is the preeminent factor in determining the forecast skill for the large-scale circulation as well as for metrics such as hurricane track forecasts that depend closely on the prediction skill of the large-scale flow.

These results are for hindcasts, but the ACC and RMSE for our real-time forecasts are nearly identical. An important caveat is that the operational GFS supports nearly the entire NCEP modeling suite, and so the GFS has many more demands and a much more stringent evaluation process imposed upon its development than does SHiELD. The development cycle of the GFS will therefore necessarily be less rapid and more methodological than that of SHiELD. Alternately, an experimental research model like SHiELD does have the freedom to pursue many different avenues for model development (“failure is always an option”) so that the most successful new ideas can later be transitioned into operations, a major goal of the UFS.

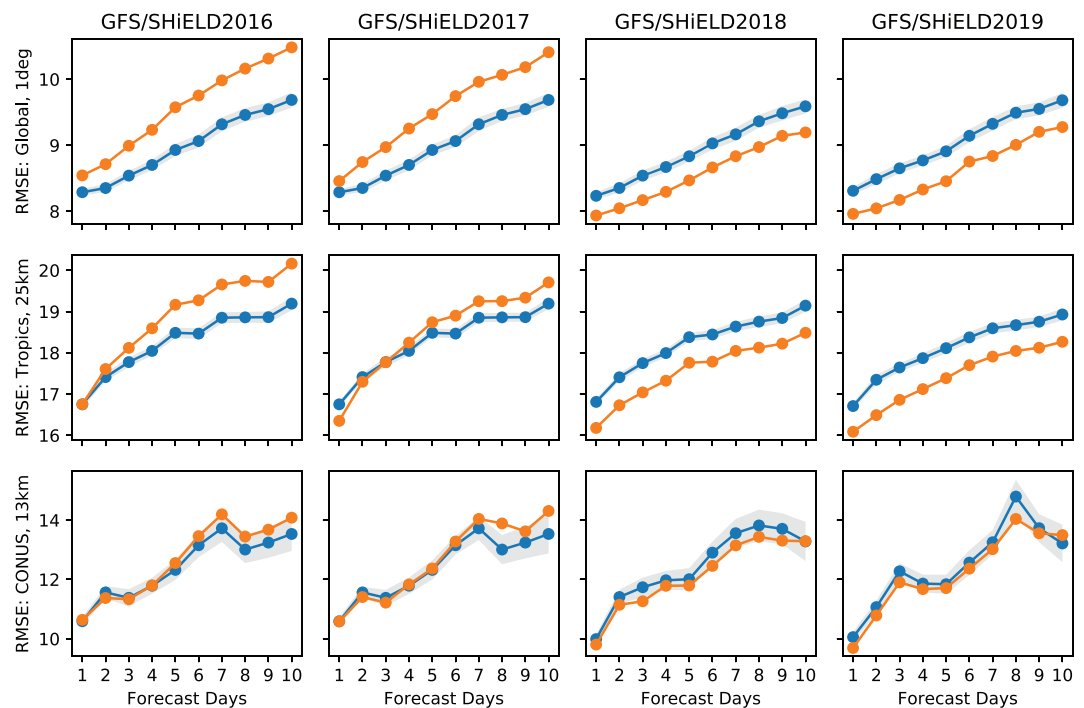


Figure 5. RMSE of 24-hr precipitation (mm) for different versions of 13-km SHiELD (orange) compared to contemporary GFS (blue). Each version’s results are aggregated over the same 2-year of hindcast periods plotted in Figures 3 and 4. (top row) Global verification versus GPCP data set (regridged to 1°); (middle row) tropics (30°S to 30°N) verification versus TRMM data set (regridged to 25 km); and (bottom row) CONUS verification versus StageIV data set (regridged to 13 km). Gray shading is the 95% confidence interval.

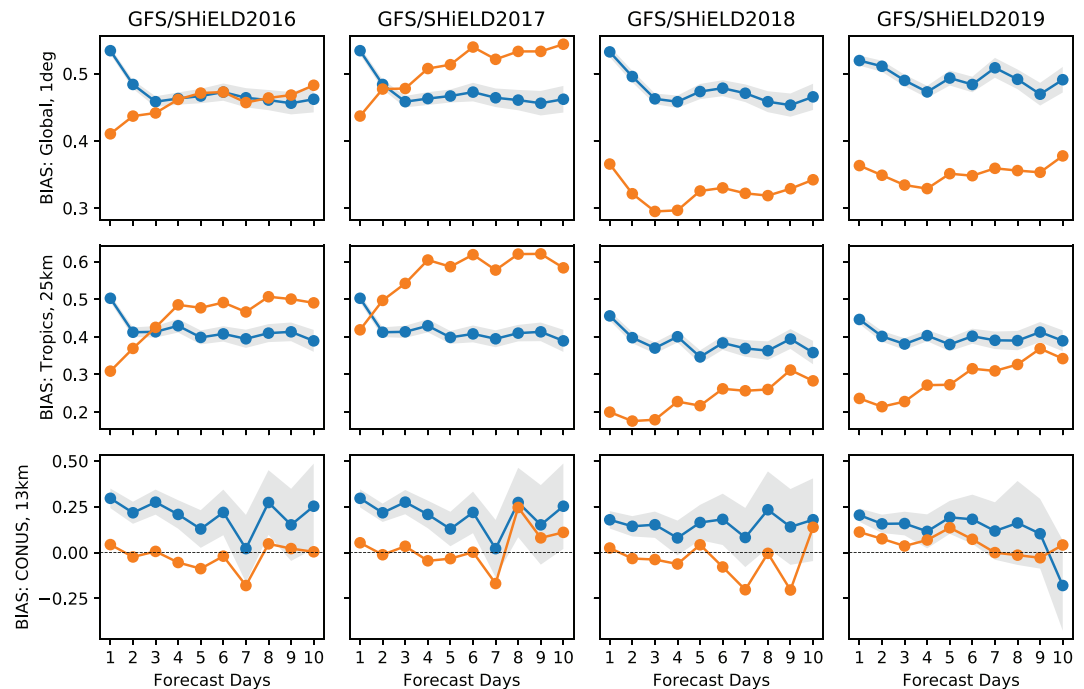


Figure 6. As in Figure 5 but for precipitation bias (mm day^{-1}), the arithmetic difference between means from the model and observations. Negative values imply too little mean precipitation.

Precipitation RMSE and biases have also improved during SHIELD development. The 2018 version significantly reduced both RMSE (Figure 5) and Bias (arithmetic difference between time-mean model and observed precipitation; Figure 6) at all lead times compared to earlier versions. Prediction of CONUS precipitation is more challenging given the smaller area and larger seasonal cycle, but RMSE still improves every year, and there is nearly no bias, especially in the 2019 version. Zhou et al. (2019) give a more thorough description of precipitation forecast skill, including other metrics. Probability distribution functions of precipitation (Figure 7) show that all of the versions depicted here have a low bias in the frequency of moderate precipitation and a high bias of both light and heavy precipitation rates compared to data from the Tropical Rainfall Measurement Mission (TRMM), although versions of SHIELD using the GFDL microphysics (2017 and later) modestly alleviate these biases. Both the GFS and all versions of 13-km SHIELD capture the observed CONUS probability distribution function very well.

Another sensible weather metric is the 2-m temperature, which has an interesting development history (Figure 8). The initial 2016 version of SHIELD had a very small warm bias, significantly less than the small (0.3 K) warm bias of the operational GFS. The 2018 version of SHIELD, which otherwise had significant improvements in other skill metrics, developed a cool bias which increased to 0.6 K by Day 10. Investigation traced the cool bias to two sources: the switch from the hybrid EDMF PBL to YSU, which by default has significantly less near-surface mixing and thereby allows the surface to cool too much, and the change in how cloud droplets absorb radiation when the Inline GFDL Microphysics was introduced. In 2019, the cloud-radiation interactions were significantly revised, and the background diffusion in the YSU PBL was increased, which significantly reduced both the cold bias and the error in 2-m temperature. The cold bias in SHIELD 2019 ranges from 0.1 K on the first day to 0.35 K on Day 10, which is approximately equal to the positive bias of the operational GFS.

3.2. T-SHIELD North Atlantic Nest for Tropical Cyclone Prediction

T-SHIELD uses the variable-resolution capabilities of FV3 to replicate the tropical cyclone track skill of global models and the intensity skill of convective-scale regional hurricane models. This configuration uses the 13-km SHIELD grid and then places a large factor of 4 two-way nest over the tropical North Atlantic (Figure 1). The resulting nested domain has grid cells of about 3-km width and interacts with its parent global domain. Earlier experiments and a comprehensive evaluation of T-SHIELD 2017 were described in

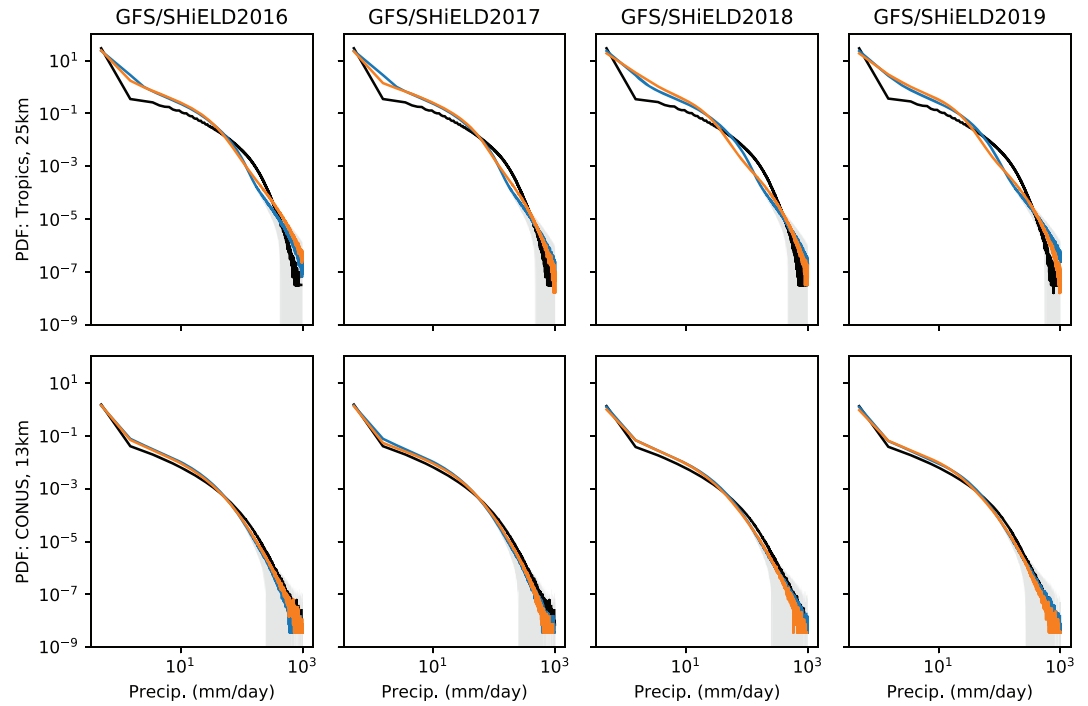


Figure 7. Precipitation PDF for 13-km SHIELD (orange) compared to contemporary GFS (blue). (top) Tropical (30°S to 30°N) precipitation versus TRMM (black). (bottom) CONUS precipitation versus StageIV (black).

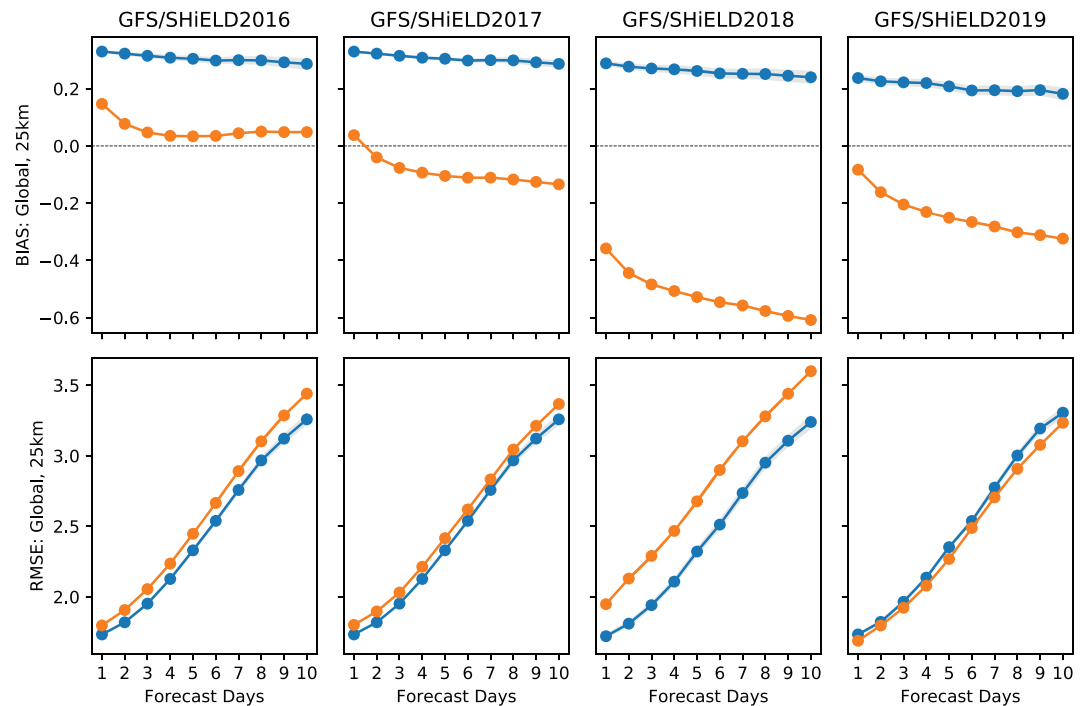


Figure 8. Global 2-m temperature (deg K) bias (top) and RMSE (bottom) for 13-km SHIELD (orange) compared to contemporary GFS (blue), both validated against ERA5 Reanalysis (Hersbach et al., 2020).

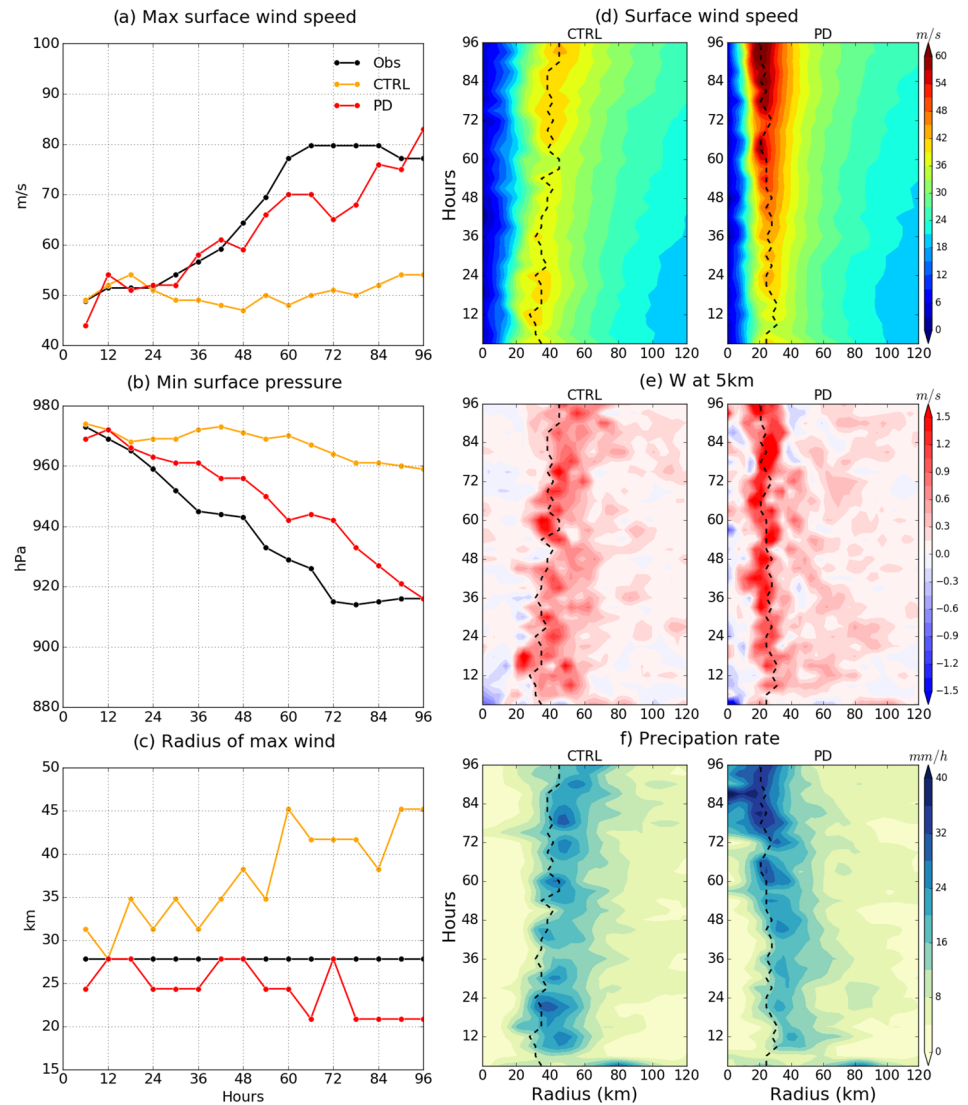


Figure 9. Hurricane Irma (2017) forecast initialized at 00 UTC 3 September 2017. Left column shows time series plots of maximum 10-m winds (a), minimum central pressure (b), and RMW (c) compared against extended Best Track observations (Demuth et al., 2006). Right column shows time-radius plots of azimuthally averaged (d) 10-m winds, (e) 5-km vertical velocity, and (f) precipitation rate from forecasts of Hurricane Irma initialized 3 September 2017, from a prototype of T-SHiELD 2018 with the monotonic (CTRL) and positive-definite tracer advection schemes (PD). The RMW is denoted as a dashed black line. Note that a localized extremum (left panels) may not be visible in the azimuthal averages (right panel), especially during rapid intensification.

Hazelton, Bender, et al. (2018) and Hazelton, Harris, and Lin (2018). T-SHiELD has been used as the initial prototype for the HAFS (Hazelton et al., 2020). Here we will describe further evolution of T-SHiELD, including progress toward rectifying two forecast issues in T-SHiELD 2017: an underintensification bias for rapidly intensifying storms and storms with a radius of maximum winds (RMW) that is too large. Note that there is no 2019 version of T-SHiELD.

Hazelton, Harris, and Lin (2018) found that the RMW in T-SHiELD 2017 was often larger than observed and in particular larger than that in HWRF simulations from the same set of cases. Zhang et al. (2015) found that reducing the parameterized mixing in the PBL scheme reduced the size of the RMW in HWRF. While reducing the parameterized mixing in the hybrid EDMF scheme gave modest improvement to hurricane structure in T-SHiELD, there was no appreciable reduction in the size of the eyewall. A dramatic and immediate impact was instead found by using the PD advection scheme for water vapor and

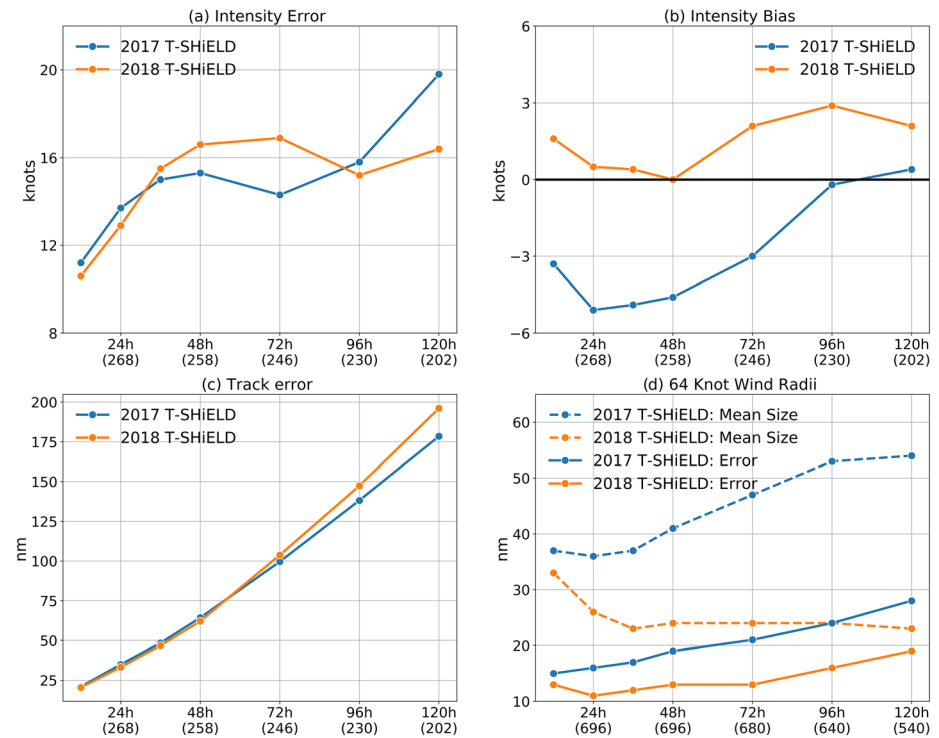


Figure 10. Verification of T-SHIELD 2017 and 2018 during the 2017 Atlantic hurricane season against the Best Track data set: intensity (a) error and (b) bias; (c) track error; and (d) 64-kt (33 m s^{-1} , hurricane-force) radii. Units shown (kt, nautical miles) are standard for U.S. operational prediction. In (a)–(c), the number of cases (individual storms) available at each lead time is shown in parentheses; in (d), the number in parentheses is the number of storm quadrants available for validation.

microphysical tracers. Results from T-SHIELD 2018 simulations of Major Hurricane Irma, initialized prior to its rapid intensification, show that a simulation using the older monotonic advection scheme (Figure 9) produces a gradually expanding vortex that does not intensify. Meanwhile, the simulation with the new PD scheme and *no other changes to the physics or dynamics, including advection of dynamical quantities*, produces an intensifying storm with a contracting eyewall. Notably, the vertical velocity within the eyewall is much more coherent with the PD scheme and is continually displaced within the eyewall, which we suspect may be driving both the intensification of Irma and a continued contraction of the eye, as well as contributing to enhanced precipitation within the eyewall. For this reason, the PD advection scheme was selected for T-SHIELD 2018.

A more systematic comparison of wind radii between the 2017 and 2018 T-SHIELD versions (Figure 10d) shows that the effect of the PD scheme is not limited to a single storm. Noting that the difference between the two T-SHIELD versions is more than just the PD scheme, we do see a systematic and substantial decrease in the radius of the 64-kt (33 m s^{-1} , hurricane force) winds in the 2018 version. The 2018 version spins up the vortex such that within 36 hr of initialization, the 64-kt radii reduce to and then remain at a consistent 20–25 nautical miles (nm; 37–46 km) for the rest of the forecast period. This represents a reduction of more than half at 120-hr lead time compared to the 2017 version, which steadily widens the 64-kt radii during the simulation. There is also a reduction in radii forecast errors compared to Best Track estimates in T-SHIELD 2018, with the qualification that there is considerable (potentially 40% for 64 kt; Landsea & Franklin, 2013) uncertainty in estimates of wind radii. This uncertainty can impact the initialization of tropical cyclones using real-time storm message files (Bender et al., 2017) and thereby of estimates of size-related impacts like precipitation and extreme winds.

The multiple changes in the 2018 version of T-SHIELD combined to create tropical cyclones which are stronger overall (Figures 10a and 10b), with little to no bias toward more intense storms at all lead times. There is a minor degradation in track error in the 2018 version at longer lead times (Figure 10c). The adoption of the

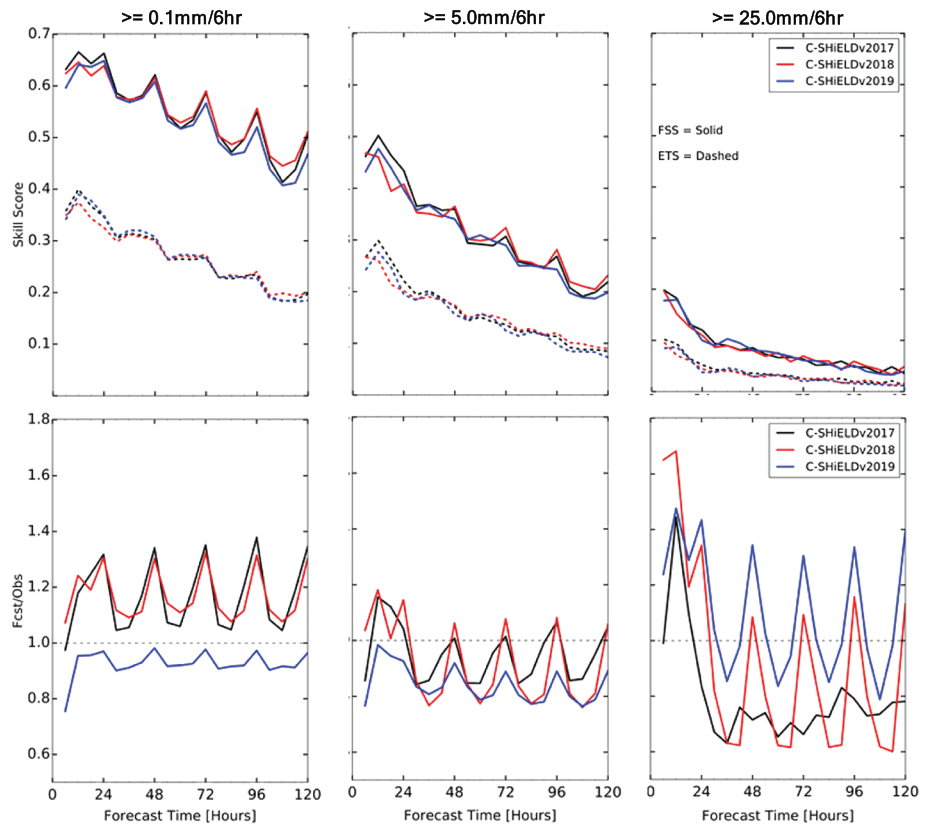


Figure 11. Precipitation skill scores (top) and bias score (bottom) versus StageIV for 6-hr CONUS precipitation in three versions of C-SHiELD, given for precipitation events greater than three 6-hourly accumulation thresholds (0.1, 5.0, and 25.0 mm). Skill scores are given for both Equitable Threat Score (ETS; Hogan & Mason, 2012) and Fractions Skill Score (FSS; Roberts & Lean, 2008). C-SHiELD 2017 is validated from May 2017 to May 2018; C-SHiELD 2018 is validated from April 2018 to May 2019; C-SHiELD 2019 is validated from January to December 2019. Validation is performed on the 4-km StageIV grid using 3×3 neighborhoods, corresponding to a 12-km radius.

PD scheme and YSU PBL scheme likely created forecasts of more intense storms mitigated by the introduction of the interactive MLO. While the weak bias of the 2017 version was alleviated, intensity predictions were not appreciably improved except at 120-hr lead time and, in fact, were degraded between 36 and 72 hr after initialization. These results show once again the great challenge of improving intensity prediction. The reduction in RMWs in simulations using the PD scheme will be discussed in more detail in a forthcoming manuscript.

3.3. C-SHiELD Nest for Continental U.S. Convection

C-SHiELD was designed to efficiently reach convective-scale resolutions in a global domain, in this case to replicate the capability of regional convective-scale models for continental convection such as the 3-km North American Model (NAM) Nest and the members of the High-Resolution Ensemble Forecast. C-SHiELD also is designed to extend convective-scale forecasts beyond the 18- to 60-hr ranges of existing U.S. operational CONUS models into the medium-range time scales and beyond. The nested domain of C-SHiELD serves as a prototype for the RFS (Carley et al., 2020) and the Rapid-Refresh Forecast System (Alexander et al., 2020), both using the regional domain capability being developed within FV3.

The 2017 version of C-SHiELD is described in Harris et al. (2019). Modified versions of C-SHiELD with different microphysics and PBL schemes are described in Zhang et al. (2019) and Snook et al. (2019). C-SHiELD 2018 saw considerable updates as shown in Table 2; C-SHiELD 2019 added incremental updates, including reconfiguration of the numerical diffusion and GFDL microphysics. We will limit our discussion to the evolution of broad forecast characteristics, but we will perform year-round validation instead of restricting the

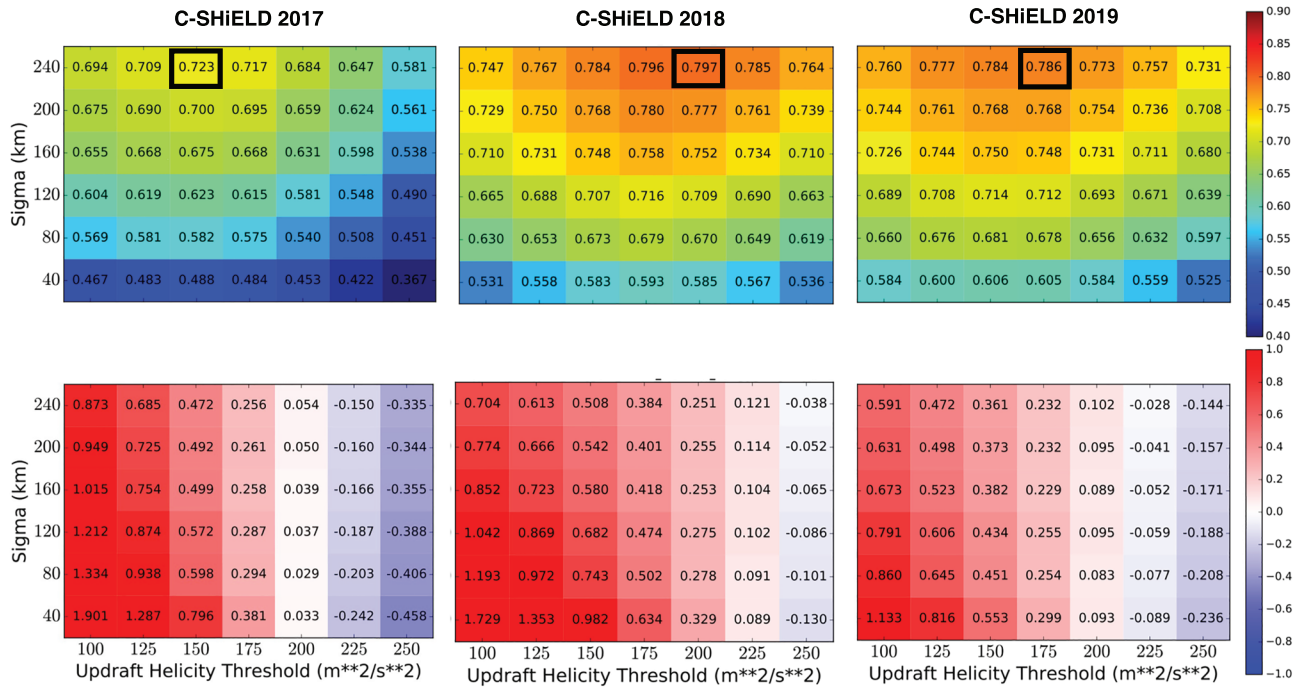


Figure 12. FSS (top) and Bias score minus 1 (bottom) for surrogate severe predictions with 12- to 36-hr lead times for three versions of C-SHiELD initialized at 00Z. Heavy black outline corresponds to the combination of UH threshold ($\text{m}^2 \text{s}^{-2}$) and smoothing radius (sigma, km) giving the highest FSS.

analysis to a single season. The time periods evaluated are given in Table 1. The exception is for the Surrogate Severe verification below, which is only verified for peak severe weather season of April to August of each year.

Precipitation forecast skill (Figure 11, top panels) is similar among all three versions of C-SHiELD. The 2019 version has the least overall bias (Figure 11, bottom panels) as earlier versions had too much light and too little heavy precipitation. The 2019 version reduced the diurnal cycle in the bias of light and moderate precipitation, although this was still apparent in the bias score for heavy precipitation and still had a prominent high bias of heavy precipitation during the first 30 hr. We speculate that the reconfiguration of the numerical diffusion, which improved storm placement, and the revised settings for the GFDL microphysics, which improved structure and evolution of the storms, combined to improve the biases in the 2019 version.

We use the surrogate severe technique of Sobash et al. (2011) to validate our 2- to 5-km updraft helicity (UH) fields against storm reports from the Storm Prediction Center. This is a well-established method used for evaluation of convective-scale prediction models (cf. https://hwt.nssl.noaa.gov/sfe/2018/docs/HWT_SFE_2018_Prelim_Findings_v1.pdf). We create surrogate severe fields and validate against observed severe fields to compute FSS and Bias scores in C-SHiELD and plot the results as a function of UH threshold and smoothing radius (Figure 12), similar to Figure 17 in Sobash et al. (2016). For all versions of C-SHiELD, the highest FSS is found from the largest smoothing radius of 240 km and for UH thresholds of 150–200 $\text{m}^2 \text{s}^{-2}$, with slightly higher or lower thresholds giving similar skill scores. The UH threshold giving the best score for C-SHiELD is higher than in many other convective-scale models due to the significantly higher updraft helicities in FV3-based models (Potvin et al., 2019). This in turn is likely due to the emphasis on vorticity in the horizontal discretization as described in Harris et al. (2019).

The maximum FSS in the 2018 and 2019 versions is about 0.8, on par with operational and research convective-scale models (cf. Sobash et al., 2019) and significantly higher than the 2017 version. There is a uniform overprediction bias for all but the highest UH thresholds (Figure 12, bottom row). This bias was significant in the 2017 version but is decreased every year for most threshold-radius combinations and for the highest-FSS combination decreases from 0.47 in 2017 to 0.22 in 2019. C-SHiELD 2019 still

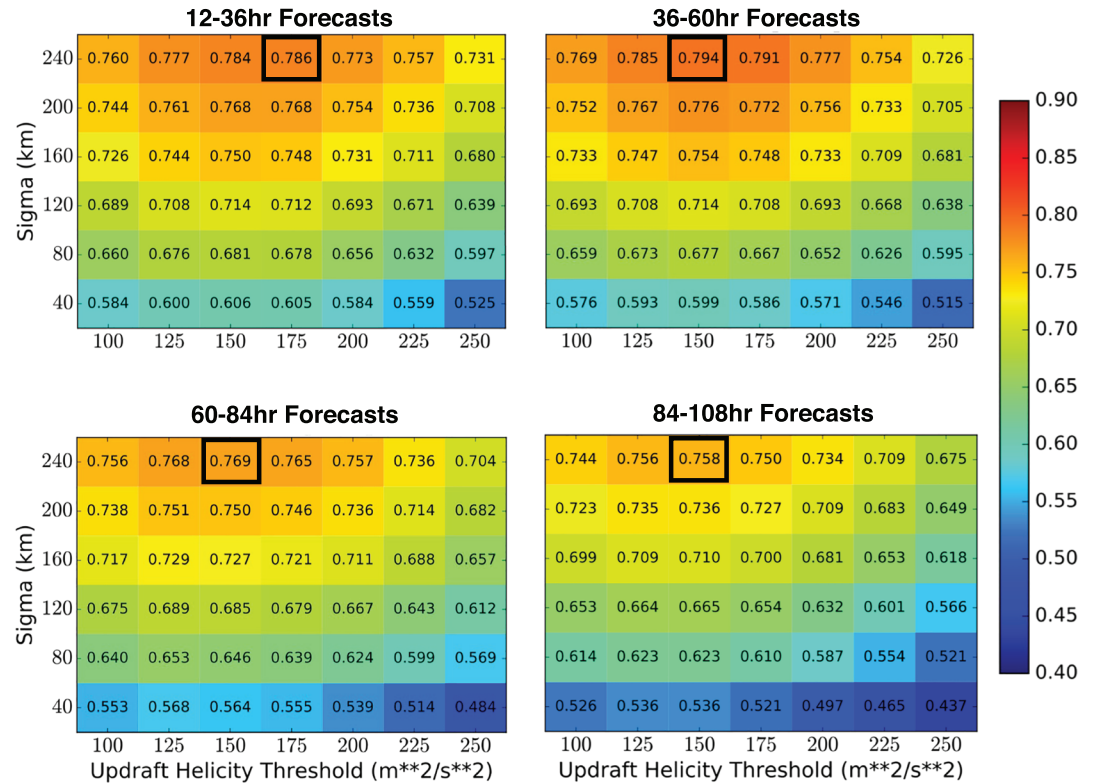


Figure 13. FSS for surrogate severe predictions at different lead times for 00Z initializations of C-SHiELD 2019.

has a high-frequency bias except for the very highest UH thresholds, as it is still too aggressive at creating strong storms.

We also investigate if skillful prediction of severe weather is possible beyond the first forecast day. Figure 13 shows surrogate severe FSS for Days 1 through 4 (Hours 12–36, 36–60, 60–84, and 84–108, respectively). The FSS value is not as high on later days as on the first, but even on Day 4, the FSS is still a respectable 0.74, indicating that there is skill in predicting severe weather multiple days in advance. These high skill scores may be partially due to the relatively large smoothing radius of 240 km.

These multiple-day severe weather forecasts are in the spirit of the convective outlooks issued by the Storm Prediction Center (www.spc.noaa.gov/products/outlook; Edwards, 2015) based on predictions of synoptic-scale environments favorable for severe weather. The advantage of using a dynamical convective-scale prediction model on medium-range time scales is that explicit prediction of storms, instead of just environments, potentially can give forecasts of convective modes and specific hazards.

3.4. S-SHiELD S2S Prediction

We briefly describe the characteristics of the Tier-2 S-SHiELD configuration, using a 25-km grid designed for climate integrations and for subseasonal and seasonal predictions. S-SHiELD is configured similarly to the 13-km SHiELD, although SHiELD’s 2-day relaxation time scale of SSTs in the MLO toward the “frozen anomalies” is extended to 15 days in S-SHiELD. Unlike the vast majority of climate models, S-SHiELD is nonhydrostatic and uses a more sophisticated microphysics which is updated much more frequently. While these features do make S-SHiELD more expensive than analogous 25-km hydrostatic climate models (cf. Murakami et al., 2016; Roberts et al., 2018), previous experience with HiRAM (Chen & Lin, 2011, 2013; Gao et al., 2018) has shown that nonhydrostatic dynamics and better microphysical-dynamical coupling yields a better representation of mesoscale convective systems and in particular of tropical cyclones, a major emphasis of our group’s research.

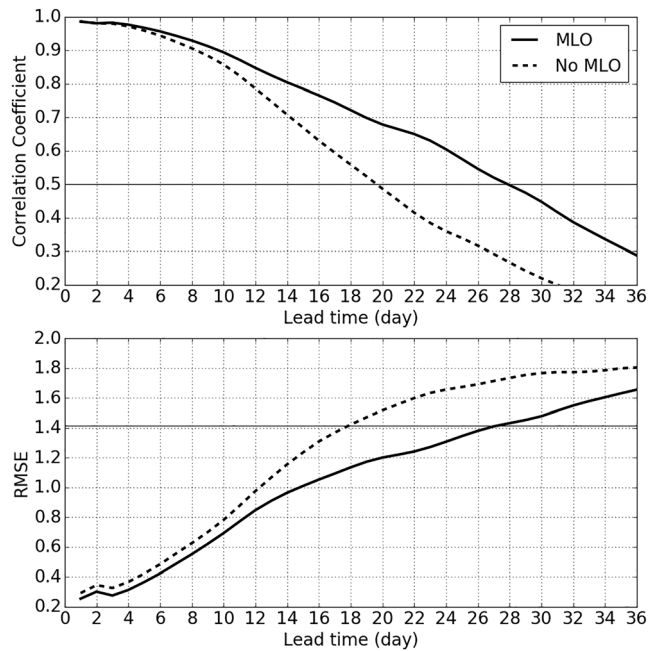


Figure 14. Prediction skill of the MJO's RMM indices in S-SHiELD with (solid) and without (dotted) the interactive MLO for ninety-two 40-day predictions initialized during the 2011–2012 DYNAMO period. (top) Correlation coefficient and (bottom) RMSE.

The MJO plays a major role in subseasonal variability but has been a challenge for many models to predict or even simulate reasonably (Kim et al., 2018). To explore the MJO prediction skill of S-SHiELD, we performed ninety-two 40-day predictions, one initialized at 00Z every 2 days from 1 October 2011 to 31 March 2012, covering the active Dynamics of the MJO (DYNAMO; Yoneyama et al., 2013) observation period. The Real-time Multivariate MJO Index (RMM; Wheeler & Hendon, 2004) is calculated for the hindcasts following the methodology of Xiang et al. (2015) and Vitart et al. (2017). For each hindcast, we compute daily-mean anomalies of outgoing longwave radiation and zonal wind at 200 mb (U200) and 850 mb (U850), averaged between 15°S and 15°N. These forecast anomalies are not bias corrected since we use observed climatology as reference instead of model climatology. We then subtract the averaged anomalies of the previous 120 days from the total anomalies to remove the signals of interannual and longer time scale variability; observed anomalies are appended to the anomalies in the hindcast. The normalized U200, U850, and outgoing longwave radiation anomalies are then projected onto the precomputed Empirical Orthogonal Functions from Wheeler and Hendon (2004) to obtain the two RMM indices.

We find that S-SHiELD with the MLO (Figure 14) has good skill (correlation > 0.7) out to 19 days and useful skill (correlation > 0.5) out to 28 days. The RMSE likewise shows similar skill (RMSE < $\sqrt{2}$ out to 27 days). This skill may not be representative of other time periods given that skill is known to be higher during strong events (cf. Xiang et al., 2015) and the period of evaluation is relatively short. However, this result does give us

confidence that S-SHiELD simulates the MJO well enough for useful S2S prediction. We plan to expand our evaluation of the MJO in forthcoming work.

The behavior of the MJO in GFDL's CMIP6-generation climate models (Zhao et al., 2018) suggests that the two keys for a good MJO simulation are an appropriate convection scheme and some form of interactive ocean, a result found also by DeMott et al. (2019) and others. A second set of S-SHiELD experiments was performed using specified climatological SSTs plus frozen anomalies. These simulations without the interactive MLO had much smaller RMM correlations, with predictions no longer useful after Day 20, and larger errors. The effect of the interactive ocean is made clear in Figure 15, in which S-SHiELD with the MLO correctly predicted the formation of all three strong MJO events during this period 10–15 days in advance and correctly propagated all events through the Maritime Continent (near 120°E longitude), although the propagation speed is slower than observed and there is some disruptions near the Maritime Continent. However, S-SHiELD with prescribed SSTs has difficulty propagating the MJO through the Maritime Continent and, for the November event, creates no MJO whatsoever. The November event proves particularly challenging for S-SHiELD without the MLO as it performs poorly at a range of lead times (Figure S2) but poses no problem for S-SHiELD with the MLO. It is clear that the simple, inexpensive MLO used in S-SHiELD is sufficient to significantly extend the predictability of the MJO.

DeMott et al. (2019) did not describe any deficiencies of the MJO from models using a 1-D column ocean instead of a 3-D dynamical ocean, which suggests a limited role for direct feedbacks between ocean circulations and the MJO. However, they did not rule out indirect effects of the MJO on ocean circulation that could impact other S2S-time scale phenomena or MJO teleconnections. Other investigators have found that the MJO does alter ocean circulations on intraseasonal time scales, notably the result of Moum et al. (2014) found during DYNAMO. It remains to be seen whether these ocean dynamical effects of the MJO are of sufficient impact to affect S2S prediction skill. One advantage of the MLO is that we can nudge to climatological SSTs and so do not have climate drifts that challenge fully coupled models.

Klingaman and DeMott (2020) found that climate models exaggerate the effect of ocean coupling on the MJO by overintensifying the MJO in El Niño years. S-SHiELD does not have a coupled dynamical ocean and nudges toward climatology and so can only represent the El Niño-Southern Oscillation state at

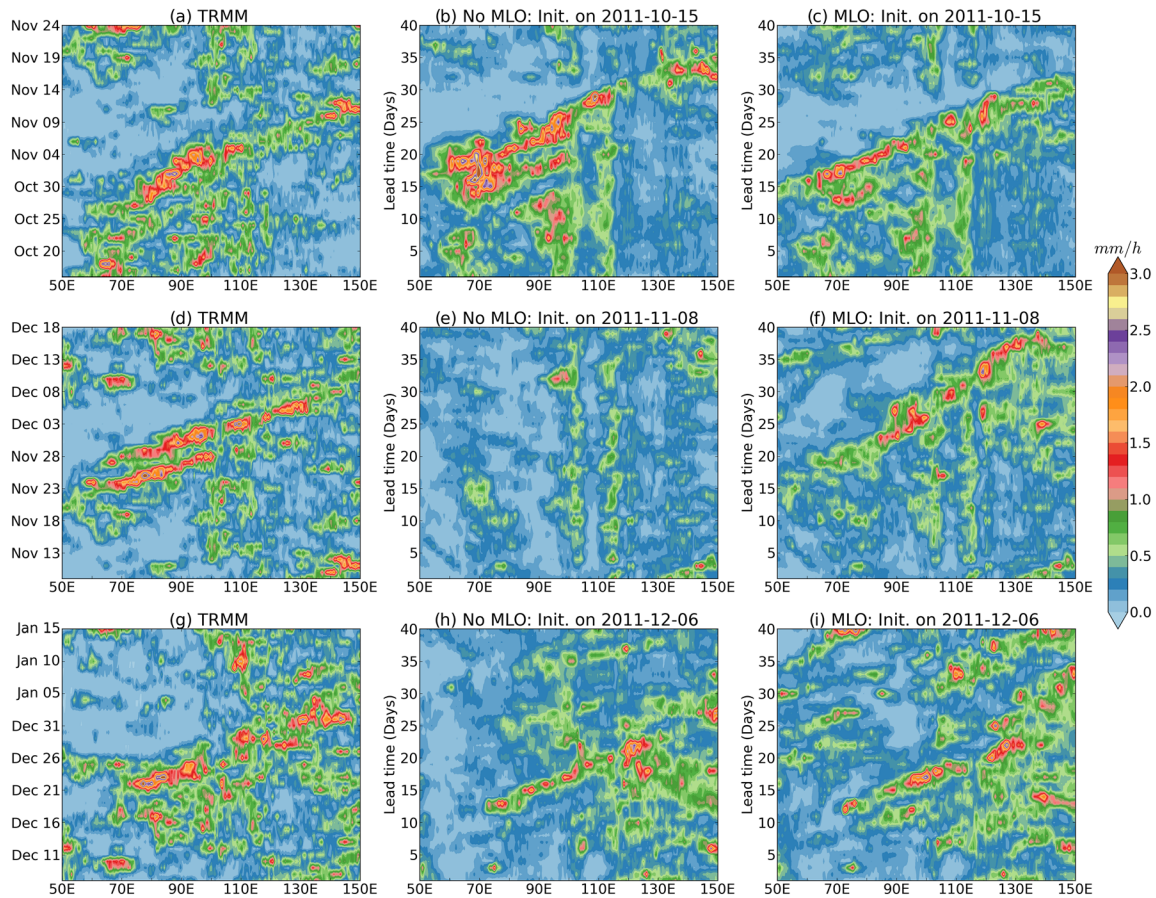


Figure 15. Precipitation (averaged from 5°S to 5°N) from TRMM (a, d, g), S-SHiELD without MLO (b, e, h), and S-SHiELD with MLO (c, f, i), for initializations at (a–c) 15 October, (d–f) 8 November, and (g–i) 6 December 2011.

initialization; indeed, the DYNAMO period was during a La Niña event (see https://origin.cpc.ncep.noaa.gov/products/analysis_monitoring/ensostuff/ONI_v5.php). Hence, this El Niño–Southern Oscillation contamination of the link between ocean coupling and the MJO is not present in S-SHiELD.

The diurnal cycle of precipitation is another challenge for climate models. Covey et al. (2016) found that nearly all climate models, even the 30-km resolution GFDL HiRAM, struggle with both the phase and amplitude of the diurnal cycle, especially over land and during boreal summer. Figure 16 presents the June–August (JJA) diurnal cycle from a 10-year S-SHiELD simulation with MLO SSTs nudged toward climatology, with results from 13-km SHiELD hindcasts shown for reference. We find that the observed phase of the diurnal cycle is beautifully matched by S-SHiELD, over both land and ocean. Most notably, the CONUS evening maximum of precipitation is reproduced. However, the amplitude of the cycle is biased low over land areas, possibly due to the inability of S-SHiELD’s 25-km grid to produce the propagating mesoscale convective systems characteristic of heavier warm-season precipitation events. This appears to be a resolution effect as 13-km SHiELD reproduces both the correct phase and amplitude of precipitation. We also find that the majority of precipitation in S-SHiELD (55% globally and 80% between 20°S and 20°N) is from the SAS convective scheme, although this does not adversely affect the phase of the diurnal cycle. S-SHiELD does have the correct phase and amplitude (albeit slightly too high) of the diurnal cycle of the 2-m temperature over land (Figure S3).

Hagos et al. (2016) found that the diurnal cycle of cloudiness and precipitation plays a key role in the propagation of the MJO through the Maritime Continent. Since S-SHiELD has considerably better diurnal cycles of precipitation and temperature over land, especially over tropical land, than do most climate models, we might expect that this improved representation of the diurnal cycle may be contributing to the improved representation of the MJO seen above.

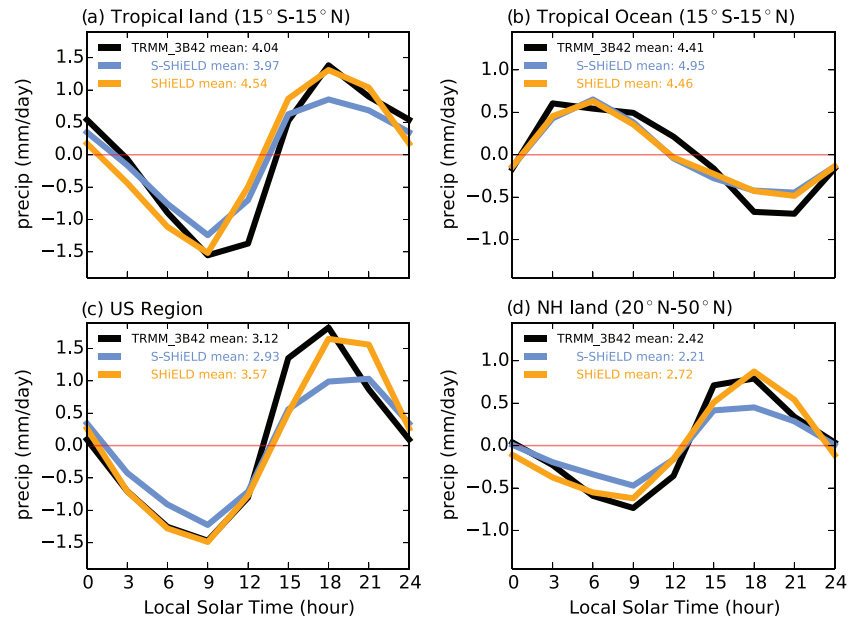


Figure 16. JJA diurnal cycle of precipitation as a function of local solar time. Shown are results from a 10-year S-SHiELD climate integration with the MLO nudged toward climatological SSTs and from Days 6–10 of 3 years of 13-km SHiELD hindcasts (initialized every 5 days), compared to TRMM 2011–2018 observations. Regions are (a) Land tropics 15°S–15°N; (b) as in (a) but only for land regions; (c) as in (a) but restricted to the contiguous U.S.; (d) as in (a) but for the Northern mid-latitudes, 20°N–50°N. Means are given in the legends as mm/day.

4. Conclusion and Prospects

We have developed the SHiELD modeling system as a research tool to demonstrate new capabilities of the FV3 Dynamical Core and of our physical parameterizations, develop new ideas in atmospheric prediction modeling, and to explore processes and phenomena within the atmosphere. Since late 2015 when FV3 was first coupled to the then-operational GFS Physics Driver, we have developed SHiELD into a promising vehicle for improving the prediction and understanding of atmospheric phenomena. SHiELD also demonstrates the potential and viability of unified modeling in which there is a single modeling system with one codebase, one executable, one preprocessor, one set of runscripts, and one set of postprocessing tools. This greatly simplifies the modeling suite and allows improvements to be exchanged between configurations.

The fundamental characteristics of SHiELD compared to previous-generation and existing operational models are documented in this and other publications. For some applications, we have previously demonstrated capabilities similar to that of existing modeling systems, such as severe-storm prediction in C-SHiELD (Harris et al., 2019) and tropical cyclone intensity prediction in T-SHiELD (Hazelton, Bender, et al., 2018; Hazelton, Harris, & Lin, 2018). We have shown significant improvements over existing models, especially over existing global models, for large-scale and hurricane prediction skill in 13-km SHiELD (Chen, Lin, Magnusson, et al., 2019; Zhou et al., 2019), and the diurnal cycle and MJO prediction in S-SHiELD. We have even shown entirely new possibilities for prediction modeling, such as skillful hurricane intensity forecasts in 13-km SHiELD (Chen, Lin, Zhou, et al., 2019), and the possibility of medium-range convective-scale prediction in C-SHiELD. *Ultimately, the true strength of SHiELD is that all of these characteristics are demonstrated in the same modeling system.*

SHiELD is designed to be an experimental research modeling system, with a particular set of scientific goals set by its developers, and thereby is more restricted in scope than the GFS, HAFS, RFS, and other general-purpose models intended for operational weather forecasting and to support broad audiences of users. While improved prediction skill is a major scientific goal and an important “vital sign” of model development, we also develop SHiELD as a means to demonstrate new modeling capabilities. SHiELD is also intended to be principally a physical atmosphere modeling system and is not intended for research into oceanic dynamics, decadal-to-centennial projection, biogeochemistry, or other topics taking place at either

longer time scales or greater complexity than SHiELD is designed for. Improvements within SHiELD can be seamlessly transitioned into other FV3-based models that do address these topics, including other UFS models and the FV3-based coupled earth-system models at GFDL, within NASA, the National Center for Atmospheric Research, and elsewhere. As such, SHiELD's progress will continue to contribute to the development and improvement of these modeling systems. SHiELD is a part of GFDL's fourth-generation modeling suite (GFDL, 2019; Figures 1 and 2) and shares common infrastructure with CM4, Earth System Model version 4, and Seamless System for Prediction and Earth System Research. SHiELD uses a different physics suite and land model from the other GFDL configurations but otherwise is constructed similarly. Advances can then be exchanged between the configurations, allowing for mutual improvement, seamless cross-time scale modeling, and potentially unification of GFDL's weather and climate modeling efforts. A significant two-way interaction between SHiELD and other UFS configurations (GFS, HAFS, RFS, etc.) is taking and promises to continue driving further improvement of all UFS applications.

Further development of SHiELD, including both FV3 and the SHiELD physics, will continue to improve the prediction skill of the configurations, address issues which have been identified, and broaden the scope toward new applications. As computing power allows, models will be pushed to higher horizontal and vertical resolution, physical processes developed to improve simulation quality and prediction skill, and to address emerging scientific questions. New capabilities within FV3, including regional and doubly periodic domains, will permit efficient simulation of processes at kilometer and subkilometer scales for basic science and for process studies to improve physical parameterizations. We are also working on a native SHiELD data assimilation cycling system to take advantage of the new advances and to create initial conditions most consistent with the forward prediction model configurations. Finally, we will continue to develop our Tier-2 configurations, with near real-time S2S predictions being made using S-SHiELD, and continued extension into the global cloud-resolving regime (cf. Stevens et al., 2019) toward new scientific problems not adequately addressed by existing regional models or by coarse-resolution global models.

Appendix A: PD Advection Scheme

The Lagrangian dynamics in FV3 uses 1-D advection operators to build the 2-D advection scheme of Lin and Rood (1996). In hydrostatic FV3, these operators are typically monotonic (Lin, 2004), in that no new extrema are created by the advection; however, monotonic advection can be overly diffusive for some applications. In nonhydrostatic FV3, the monotonicity constraint is not used for advection of dynamical quantities (vorticity, heat, and air mass), but positivity still needs to be enforced for scalar tracers. We introduce a PD scheme, which uses a weaker constraint than monotonicity which only prevents the appearance of negative values.

This positivity constraint can be applied to any scheme similar to Van Leer (1974) or the Piecewise-Parabolic Method (PPM; Colella & Woodward, 1984) in which first-guess continuous edge values $\hat{q}_{i+1/2}$ and $\hat{q}_{i-1/2}$ are interpolated from the cell-averaged values \bar{q}_i where i is a grid index. As with a standard monotonicity constraint, we break the continuity of the subgrid reconstructions across grid-cell interfaces, creating left-edge and right-edge values, Q_i^- and Q_i^+ , respectively, as well as a curvature value B_{oi} for each grid cell, which are then used to compute the flux as in Putman and Lin (2007, Appendix B).

To adjust the edge values to ensure positivity, we use the algorithm below on cell i , where notation is as in Lin (2004, Appendix A):

$$Q_i^- = \hat{q}_{i-1/2} - \bar{q}_i,$$

$$Q_i^+ = \hat{q}_{i+1/2} - \bar{q}_i,$$

$$B_{oi} = Q_i^- + Q_i^+,$$

$$\Delta A_i = Q_i^+ - Q_i^-,$$

$$A_{4i} = -3 B_{oi},$$

$$\text{If } \text{abs}(\hat{q}_{i+1/2} - \hat{q}_{i-1/2}) > -A_{4i} \text{ and } \bar{q}_i + \Delta A_i^2 / (4A_{4i}) + \frac{1}{12}A_{4i} < 0 \text{ then}$$

$$\text{If } Q_i^- Q_i^+ > 0 \text{ then}$$

$$Q_i^- = Q_i^+ = B_{oi} = 0,$$

Else if $dA_i > 0$ then

$$Q_i^+ = 2^* - Q_i^-,$$

$$B_{oi} = -Q_i^-,$$

Else

$$Q_i^- = -2^* Q_i^+,$$

$$B_{oi} = -Q_i^+.$$

Appendix B: Split and In-line GFDL Microphysics

The GFDL microphysics, a single-moment six-category microphysics, has its origin in the microphysics of Lin et al. (1983) as implemented within GFDL ZETAC (Knutson et al., 2007; Knutson & Tuleya, 2008; Pauluis & Garner, 2006) with further developments from Lord et al. (1984) and Krueger et al. (1995). It was later substantially revised for use in HiRAM (Chen & Lin, 2011, 2013; Gao et al., 2017, 2019; Harris et al., 2016) by adding the following updates:

1. Time-splitting is applied between warm-rain and ice-phase processes, with the warm-rain processes called twice per invocation.
2. PPM is applied for sedimentation of all condensate species except cloud water, ensuring shape preservation and stability.
3. The heat content of condensates is included when heating/cooling grid cells.
4. Scale awareness is achieved by assuming a horizontal subgrid distribution and a second-order vertical reconstruction for autoconversion processes with a slope which increases with grid-cell width.
5. Additional microphysical processes, including ice nucleation and cloud ice sedimentation, were introduced.

In the Split GFDL Microphysics first implemented within SHIELD, microphysical processes were divided into fast and (relatively) slow processes, where the fast processes (primarily phase changes and latent heating/cooling) are updated after the vertical remapping in FV3, while the slower processes remain in the physical driver. More recently, the entire GFDL microphysics was Inlined within the dynamical core. The advantages of Inlining are (1) to separate the physical processes based on different time scales to better interact with dynamics processes and (2) to be able to make the physical parameterization thermodynamically consistent with the dynamical core. Other updates in the Inline microphysics include a time-implicit monotonic scheme for sedimentation to ensure stability without needing to subcycle; precise conservation of the total moist energy; and transportation of heat and momentum carried by condensates during sedimentation.

Appendix C: A Note on Terminology

The term “model” means many different things in many contexts and can be confusing. In this paper, we use the term “model” only in the abstract (“other general-purpose models” and “NCEP Modeling Suite”) or as part of the name of another system (“Noah Land Surface Model” and “GFDL Hurricane Model”). For concreteness, we refer to SHIELD as a “modeling system” which can be used in a variety of “configurations” (13-km SHIELD, C-SHIELD, T-SHIELD, and S-SHIELD), each upgraded to new yearly versions (SHIELD 2016, SHIELD 2017, etc.).

Data Availability Statement

Supporting data can be found online (10.5281/zenodo.3997344).

Acknowledgments

SHIELD grew out of a major collaboration between GFDL and EMC and would not have been possible without the physical parameterization suite, software, data, and especially input initial conditions and baseline forecasts made freely available by EMC and the National Weather Service. We thank Jongil Han for providing SA-SAS and George Gayno and Helin Wei for providing EMC preprocessing tools and land model inputs and for significant assistance with these tools and data sets. We also thank James Franklin (NHC, retired) for advice on the accuracy of the wind radii in the Best Track data set. Kate Zhou and Tom Delworth provided reviews of this manuscript. Xi Chen, Linjong Zhou, Kun Gao, Yongqiang Sun, Kai-Yuan Cheng, and Morris Bender are funded under Award NA18OAR4320123 from the National Oceanic and Atmospheric Administration, U.S. Department of Commerce. Xi Chen, Zhou, and Cheng were additionally funded by the Next-Generation Global Prediction System project of the National Weather Service. The National Oceanic and Atmospheric Administration's Hurricane Supplemental Program Office partially funded Zhou, Gao, and Bender under Award NA19OAR0220147; Sun under NA19OAR0220145; and Cheng under NA19OAR0220146. We thank two anonymous reviewers for their insightful comments.

References

Adcroft, A., Anderson, W., Balaji, V., Blanton, C., Bushuk, M., Dufour, C. O., et al. (2019). The GFDL Global Ocean and Sea Ice Model OM4.0: Model Description and Simulation Features. *Journal of Advances in Modeling Earth Systems*, 11(10), 3167–3211. <https://doi.org/10.1029/2019ms001726>

Alexander, C., Carley, J., Heinselmann, P. L., & Harris, L. (2020). Advancements of the FV3 Stand-Alone Regional Model. In 100th Annual Meeting. AMS.

Alpert, J. C. (2004). Sub-grid scale mountain blocking at NCEP. In *Proceedings of 20th Conference on WAF, 16th conference on NWP*.

Arnold, N. P., & Putman, W. M. (2018). Nonrotating convective self-aggregation in a limited area AGCM. *Journal of Advances in Modeling Earth Systems*, 10, 1029–1046. <https://doi.org/10.1002/2017MS001218>

Balaji, V. (2012). The flexible modeling system. In *Earth system modelling-volume 3* (pp. 33–41). Berlin, Heidelberg: Springer. https://doi.org/10.1007/978-3-642-23360-9_5

Bender, M. A., Marchok, T., Tuleya, R. E., Ginis, I., Tallapragada, V., & Lord, S. J. (2019). Hurricane model development at GFDL: A collaborative success story from a historical perspective. *Bulletin of the American Meteorological Society*, 100(9), 1725–1736. <https://doi.org/10.1175/BAMS-D-18-0197.1>

Bender, M. A., Marchok, T. P., Sampson, C. R., Knaff, J. A., & Morin, M. J. (2017). Impact of storm size on prediction of storm track and intensity using the 2016 Operational GFDL Hurricane Model. *Weather and Forecasting*, 32(4), 1491–1508. <https://doi.org/10.1175/WAF-D-16-0220.1>

Brown, A., Milton, S., Cullen, M., Golding, B., Mitchell, J., & Shelly, A. (2012). Unified modeling and prediction of weather and climate: A 25-year journey. *Bulletin of the American Meteorological Society*, 93(12), 1865–1877. <https://doi.org/10.1175/BAMS-D-12-00018.1>

Carley, J. R., et al. (2020). Advances toward an operational convection-allowing ensemble prediction system in the Unified Forecast System at NOAA. In 100th Annual Meeting. AMS.

Chen, J. H., Chen, X., Lin, S. J., Magnusson, L., Bender, M., Zhou, L., & Rees, S. (2018). Tropical cyclones in GFDL fvGFS—Impacts of dycore, physics and initial conditions. In *33rd Conf. on Hurricane and Tropical Meteorology*.

Chen, J. H., & Lin, S. J. (2011). The remarkable predictability of inter-annual variability of Atlantic hurricanes during the past decade. *Geophysical Research Letters*, 38, L11804. <https://doi.org/10.1029/2011GL047629>

Chen, J. H., & Lin, S. J. (2013). Seasonal predictions of tropical cyclones using a 25-km-resolution general circulation model. *Journal of Climate*, 26(2), 380–398. <https://doi.org/10.1175/JCLI-D-12-00061.1>

Chen, J. H., Lin, S. J., Magnusson, L., Bender, M., Chen, X., Zhou, L., et al. (2019). Advancements in hurricane prediction with NOAA's next-generation forecast system. *Geophysical Research Letters*, 46, 4495–4501. <https://doi.org/10.1029/2019GL082410>

Chen, J. H., Lin, S. J., Zhou, L., Chen, X., Rees, S., Bender, M., & Morin, M. (2019). Evaluation of tropical cyclone forecasts in the next generation global prediction system. *Monthly Weather Review*, 147(9), 3409–3428. <https://doi.org/10.1175/MWR-D-18-0227.1>

Chun, H.-Y., & Baik, J.-J. (1998). Momentum Flux by Thermally Induced Internal Gravity Waves and Its Approximation for Large-Scale Models. *Journal of the Atmospheric Sciences*, 55(21), 3299–3310. [https://doi.org/10.1175/1520-0469\(1998\)055<3299:mfbtti>2.0.co;2](https://doi.org/10.1175/1520-0469(1998)055<3299:mfbtti>2.0.co;2)

Clough, S., Shephard, M., Mlawer, E., Delamere, J., Iacono, M., Cady-Pereira, K., et al. (2005). Atmospheric radiative transfer modeling: A summary of the AER codes. *Journal of Quantitative Spectroscopy and Radiative Transfer*, 91(2), 233–244. <https://doi.org/10.1016/j.jqsrt.2004.05.058>

Colella, P., & Woodward, P. R. (1984). The piecewise parabolic method (PPM) for gas-dynamical simulations. *Journal of Computational Physics*, 54(1), 174–201. [https://doi.org/10.1016/0021-9991\(84\)90143-8](https://doi.org/10.1016/0021-9991(84)90143-8)

Covey, C., Gleckler, P. J., Doutriaux, C., Williams, D. N., Dai, A., Fasullo, J., et al. (2016). Metrics for the diurnal cycle of precipitation: Toward routine benchmarks for climate models. *Journal of Climate*, 29(12), 4461–4471. <https://doi.org/10.1175/JCLI-D-15-0664.1>

de Boyer Montégut, C., Madec, G., Fischer, A. S., Lazar, A., & Iudicone, D. (2004). Mixed layer depth over the global ocean: An examination of profile data and a profile-based climatology. *Journal of Geophysical Research*, 109, C12003. <https://doi.org/10.1029/2004JC002378>

Delworth, T. L., Cooke, W. F., Adcroft, A., Bushuk, M., Chen, J. H., Dunne, K. A., et al. (2020). SPEAR—The next generation GFDL modeling system for seasonal to multidecadal prediction and projection. *Journal of Advances in Modeling Earth Systems*, 12, e2019MS001895. <https://doi.org/10.1029/2019MS001895>

DeMott, C. A., Klingaman, N. P., Tseng, W.-L., Burt, M. A., Gao, Y., & Randall, D. A. (2019). The convection connection: How ocean feedbacks affect tropical mean moisture and MJO propagation. *Journal of Geophysical Research: Atmospheres*, 124, 11,910–11,931. <https://doi.org/10.1029/2019JD031015>

Demuth, J. L., DeMaria, M., & Knaff, J. A. (2006). Improvement of advanced microwave sounding unit tropical cyclone intensity and size estimation algorithms. *Journal of Applied Meteorology and Climatology*, 45(11), 1573–1581. <https://doi.org/10.1175/JAM2429.1>

Dong, J., Liu, B., Zhang, Z., Wang, W., Mehra, A., Hazelton, A. T., et al. (2020). The evaluation of Real-Time Hurricane Analysis and Forecast System (HAFS) Stand-Alone Regional (SAR) model performance for the 2019 Atlantic hurricane season. *Atmosphere*, 11(6), 617. <https://doi.org/10.3390/atmos11060617>

Dunne, J. P., Horowitz, L. W., Adcroft, A. J., Ginoux, P., Held, I. M., John, J. G., et al. (2020). The GFDL Earth System Model version 4.1 (GFDL-ESM 4.1): Overall coupled model description and simulation characteristics. *Journal of Advances in Modeling Earth Systems*, 12, e2019MS002015. <https://doi.org/10.1029/2019MS002015>

ECMWF. (2019a). Part III: Dynamics and numerical procedures. IFS Documentation CY46R1.

ECMWF. (2019b). Part IV: Physical processes. IFS Documentation CY46R1.

Edwards, R. (2015). Overview of the storm prediction center. In 13th History Symposium.

Ek, M. B., Mitchell, K. E., Lin, Y., Rogers, E., Grunmann, P., Koren, V., et al. (2003). Implementation of Noah land surface model advances in the National Centers for Environmental Prediction operational mesoscale Eta model. *Journal of Geophysical Research*, 108(D22), 8851. <https://doi.org/10.1029/2002JD003296>

Gao, K., Chen, J. H., Harris, L., Sun, Y., & Lin, S. J. (2019). Skillful prediction of monthly major hurricane activity in the North Atlantic with two-way nesting. *Geophysical Research Letters*, 46, 9222–9230. <https://doi.org/10.1029/2019GL083526>

Gao, K., Chen, J. H., Harris, L. M., Lin, S. J., Xiang, B., & Zhao, M. (2017). Impact of intraseasonal oscillations on the tropical cyclone activity over the Gulf of Mexico and western Caribbean Sea in GFDL HiRAM. *Journal of Geophysical Research: Atmospheres*, 122, 13–125. <https://doi.org/10.1002/2017JD027756>

GFDL. (2019). The 5–10 year strategic plan. Available at https://www.gfdl.noaa.gov/wp-content/uploads/2019/10/2019_GFDL_External_Review_Strategic_Plan.pdf

Guo, Y., Yu, Y., Lin, P., Liu, H., He, B., Bao, Q., et al. (2020). Overview of the CMIP6 Historical Experiment Datasets with the Climate System Model CAS FGOALS-f3-L. *Advances in Atmospheric Sciences*, 37(10), 1057–1066. <https://doi.org/10.1007/s00376-020-2004-4>

- Haarsma, R., van der Linden, E. C., Selten, F., & van der Schrier, G. (2017). Extreme future central European droughts in a high-resolution global climate model. In *EGU General Assembly Conference Abstracts* (Vol. 19, p. 14128).
- Hagos, S. M., Zhang, C., Feng, Z., Burleyson, C. D., De Mott, C., Kerns, B., et al. (2016). The impact of the diurnal cycle on the propagation of Madden-Julian Oscillation convection across the Maritime Continent. *Journal of Advances in Modeling Earth Systems*, *8*, 1552–1564. <https://doi.org/10.1002/2016MS000725>
- Han, J., & Pan, H.-L. (2011). Revision of convection and vertical diffusion schemes in the NCEP Global Forecast System. *Weather and Forecasting*, *26*(4), 520–533. <https://doi.org/10.1175/WAF-D-10-05038.1>
- Han, J., Wang, W., Kwon, Y. C., Hong, S.-Y., Tallapragada, V., & Yang, F. (2017). Updates in the NCEP GFS cumulus convection schemes with scale and aerosol awareness. *Weather and Forecasting*, *32*.
- Han, J., Witek, M. L., Teixeira, J., Sun, R., Pan, H., Fletcher, J. K., & Bretherton, C. S. (2016). Implementation in the NCEP GFS of a hybrid eddy-diffusivity mass-flux (EDMF) boundary layer parameterization with dissipative heating and modified stable boundary layer mixing. *Weather and Forecasting*, *31*(1), 341–352. <https://doi.org/10.1175/WAF-D-15-0053.1>
- Harris, L. M., & Lin, S.-J. (2014). Global-to-Regional Nested Grid Climate Simulations in the GFDL High Resolution Atmospheric Model. *Journal of Climate*, *27*(13), 4890–4910. <https://doi.org/10.1175/jcli-d-13-00596.1>
- Harris, L., Lin, S. J., & Chen, J. H. (2014, May). Great Plains warm-season precipitation in a two-way nested high-resolution GCM. In *EGU General Assembly Conference Abstracts* (Vol. 16).
- Harris, L. M., & Lin, S. J. (2013). A two-way nested global-regional dynamical core on the cubed-sphere grid. *Monthly Weather Review*, *141*(1), 283–306. <https://doi.org/10.1175/MWR-D-11-00201.1>
- Harris, L. M., Lin, S. J., & Tu, C. (2016). High-resolution climate simulations using GFDL HIRAM with a stretched global grid. *Journal of Climate*, *29*(11), 4293–4314. <https://doi.org/10.1175/JCLI-D-15-0389.1>
- Harris, L. M., Rees, S. L., Morin, M., Zhou, L., & Stern, W. F. (2019). Explicit prediction of continental convection in a skillful variable-resolution global model. *Journal of Advances in Modeling Earth Systems*, *11*, 1847–1869. <https://doi.org/10.1029/2018MS001542>
- Hazelton, A., et al. (2020). The global-nested Hurricane Analysis and Forecast System (HAFS): Results from the 2019 Atlantic hurricane season. In 100th Annual Meeting. AMS.
- Hazelton, A. T., Bender, M., Morin, M., Harris, L., & Lin, S. J. (2018). 2017 Atlantic hurricane forecasts from a high-resolution version of the GFDL fvGFS model: Evaluation of track, intensity, and structure. *Weather and Forecasting*, *33*(5), 1317–1337. <https://doi.org/10.1175/WAF-D-18-0056.1>
- Hazelton, A. T., Harris, L., & Lin, S. J. (2018). Evaluation of tropical cyclone structure forecasts in a high-resolution version of the multi-scale GFDL fvGFS model. *Weather and Forecasting*, *33*(2), 419–442. <https://doi.org/10.1175/WAF-D-17-0140.1>
- Held, I. M., Guo, H., Adcroft, A., Dunne, J. P., Horowitz, L. W., Krasting, J., et al. (2019). Structure and performance of GFDL's CM4.0 climate model. *Journal of Advances in Modeling Earth Systems*, *11*, 3691–3727. <https://doi.org/10.1029/2019MS001829>
- Held, I. M., Zhao, M., & Wyman, B. (2007). Dynamic radiative-convective equilibria using GCM column physics. *Journal of the Atmospheric Sciences*, *64*(1), 228–238. <https://doi.org/10.1175/JAS3825.11>
- Hersbach, H., Bell, B., Berrisford, P., Hirahara, S., Horányi, A., Muñoz-Sabater, J., et al. (2020). The ERA5 global reanalysis. *Quarterly Journal of the Royal Meteorological Society*, *146*(730), 1999–2049. <https://doi.org/10.1002/qj.3803>
- Hogan, R. J., & Mason, I. J. (2012). Deterministic forecasts of binary events. In I. T. Jolliffe & D. B. Stephenson (Eds.), *Forecast verification: A practitioner's guide in atmospheric science* (2nd ed., pp. 31–59). Wiley. Retrieved from <https://onlinelibrary.wiley.com/doi/book/10.1002/9781119960003>
- Hong, S.-Y. (2010). A new stable boundary-layer mixing scheme and its impact on the simulated East Asian summer monsoon. *Quarterly Journal of the Royal Meteorological Society*, *136*(651), 1481–1496. <https://doi.org/10.1002/qj.665>
- Hong, S. Y., Noh, Y., & Dudhia, J. (2006). A new vertical diffusion package with an explicit treatment of entrainment processes. *Monthly Weather Review*, *134*(9), 2318–2341. <https://doi.org/10.1175/MWR3199.1>
- Jeevanjee, N. (2017). Vertical velocity in the gray zone. *Journal of Advances in Modeling Earth Systems*, *9*, 2304–2316. <https://doi.org/10.1002/2017MS001059>
- Kim, H., Vitart, F., & Waliser, D. E. (2018). Prediction of the Madden-Julian Oscillation: A review. *Journal of Climate*, *31*(23), 9425–9443. <https://doi.org/10.1175/JCLI-D-18-0210.1>
- Klingaman, N. P., & DeMott, C. A. (2020). Mean-state biases and interannual variability affect perceived sensitivities of the Madden-Julian oscillation to air–sea coupling. *Journal of Advances in Modeling Earth Systems*, *12*, e2019MS001799. <https://doi.org/10.1029/2019MS001799>
- Knutson, T. R., Sirutis, J. J., Garner, S. T., Held, I. M., & Tuleya, R. E. (2007). Simulation of the recent multidecadal increase of Atlantic hurricane activity using an 18-km-grid regional model. *Bulletin of the American Meteorological Society*, *88*(10), 1549–1565. <https://doi.org/10.1175/BAMS-88-10-1549>
- Knutson, T. R., & Tuleya, R. E. (2008). *Tropical cyclones and climate change: Revisiting recent studies at GFDL* (pp. 120–144). Cambridge, UK: Cambridge University Press.
- Krueger, S. K., Fu, Q., Liou, K. N., & Chin, H. N. S. (1995). Improvements of an ice-phase microphysics parameterization for use in numerical simulations of tropical convection. *Journal of Applied Meteorology*, *34*(1), 281–287. <https://doi.org/10.1175/1520-0450-34.1.281>
- Landsea, C. W., & Franklin, J. L. (2013). Atlantic hurricane database uncertainty and presentation of a new database format. *Monthly Weather Review*, *141*(10), 3576–3592. <https://doi.org/10.1175/MWR-D-12-00254.1>
- Lin, S. J. (2004). A “vertically Lagrangian” finite-volume dynamical core for global models. *Monthly Weather Review*, *132*(10), 2293–2307. [https://doi.org/10.1175/1520-0493\(2004\)132<2293:AVLFDC>2.0.CO;2](https://doi.org/10.1175/1520-0493(2004)132<2293:AVLFDC>2.0.CO;2)
- Lin, S.-J., Harris, L. M., Benson, R., Zhou, L., Chen, J.-H., & Chen, X. (2017). Towards a unified prediction system from weather to climate scale. *Second Symposium on Multi-Scale Atmospheric Predictability*, Seattle, WA, Paper, 3, 1.
- Lin, S.-J., & Rood, R. B. (1996). Multidimensional Flux-Form Semi-Lagrangian Transport Schemes. *Monthly Weather Review*, *124*(9), 2046–2070. [https://doi.org/10.1175/1520-0493\(1996\)124<2046:mffsllt>2.0.co;2](https://doi.org/10.1175/1520-0493(1996)124<2046:mffsllt>2.0.co;2)
- Lin, Y. L., Farley, R. D., & Orville, H. D. (1983). Bulk parameterization of the snow field in a cloud model. *Journal of Climate and Applied Meteorology*, *22*(6), 1065–1092. [https://doi.org/10.1175/1520-0450\(1983\)022<1065:BPOTSF>2.0.CO;2](https://doi.org/10.1175/1520-0450(1983)022<1065:BPOTSF>2.0.CO;2)
- Lord, S., Willoughby, H. E., & Piotrowicz, J. M. (1984). Role of a parameterized ice-phase microphysics in an axisymmetric, nonhydrostatic tropical cyclone model. *Journal of the Atmospheric Sciences*, *41*(19), 2836–2848. [https://doi.org/10.1175/1520-0469\(1984\)041<2836:ROAPIP>2.0.CO;2](https://doi.org/10.1175/1520-0469(1984)041<2836:ROAPIP>2.0.CO;2)
- Marchok, T., Morin, M. J., Knaff, J., Sampson, C. R., Hazelton, A., & Lin, S. J. (2018). An evaluation of surface wind structure forecasts from the fvGFS and operational dynamical models. In *33rd Conference on Hurricanes and Tropical Meteorology*. AMS.

- McCormack, J. P., Eckermann, S. D., Siskind, D. E., & McGee, T. J. (2006). CHEM2D-OPP: A new linearized gas-phase ozone photochemistry parameterization for high-altitude NWP and climate models. *Atmospheric Chemistry and Physics*, 6(12), 4943–4972. <https://doi.org/10.5194/acp-6-4943-2006>
- McGregor, J. L. (2015). Recent developments in variable-resolution global climate modelling. *Climatic Change*, 129(3–4), 369–380. <https://doi.org/10.1007/s10584-013-0866-5>
- Moum, J. N., de Zoete, S. P., Smyth, W. D., Edson, J. B., DeWitt, H. L., Moulin, A. J., et al. (2014). Air–sea interactions from westerly wind bursts during the November 2011 MJO in the Indian Ocean. *Bulletin of the American Meteorological Society*, 95(8), 1185–1199. <https://doi.org/10.1175/BAMS-D-12-00225.1>
- Murakami, H., Vecchi, G. A., Villarini, G., Delworth, T. L., Gudgel, R., Underwood, S., et al. (2016). Seasonal Forecasts of Major Hurricanes and Landfalling Tropical Cyclones using a High-Resolution GFDL Coupled Climate Model. *Journal of Climate*, 29(22), 7977–7989. <https://doi.org/10.1175/jcli-d-16-0233.1>
- NCEP (2020). List of GFS implementations. Available at https://www.emc.ncep.noaa.gov/emc/pages/numerical_forecast_systems/gfs/implementations.php. Last accessed 22 May 2020.
- Pauluis, O., & Garner, S. (2006). Sensitivity of radiative–convective equilibrium simulations to horizontal resolution. *Journal of the Atmospheric Sciences*, 63(7), 1910–1923. <https://doi.org/10.1175/JAS3705.1>
- Pollard, R. T., Rhines, P. B., & Thompson, R. (1973). The deepening of the mixed layer. *Geophysical Fluid Dynamics*, 3, 381–404.
- Potvin, C. K., Carley, J. R., Clark, A. J., Wicker, L. J., Skinner, P. S., Reinhart, A. E., et al. (2019). Systematic comparison of convection-allowing models during the 2017 NOAA HWT Spring Forecasting Experiment. *Weather and Forecasting*, 34(5), 1395–1416. <https://doi.org/10.1175/WAF-D-19-0056.1>
- Putman, W. M., & Lin, S.-J. (2007). Finite-volume transport on various cubed-sphere grids. *Journal of Computational Physics*, 227(1), 55–78. <https://doi.org/10.1016/j.jcp.2007.07.022>
- Putman, W. M., & Suarez, M. (2011). Cloud-system resolving simulations with the NASA Goddard Earth Observing System global atmospheric model (GEOS-5). *Geophysical Research Letters*, 38, L16809. <https://doi.org/10.1029/2011GL048438>
- Roberts, C. D., Senan, R., Molteni, F., Boussetta, S., Mayer, M., & Keeley, S. P. E. (2018). Climate model configurations of the ECMWF Integrated Forecasting System (ECMWF-IFS cycle 43r1) for HighResMIP. *Geoscientific Model Development*, 11(9), 3681–3712. <https://doi.org/10.5194/gmd-11-3681-2018>
- Roberts, N. M., & Lean, H. W. (2008). Scale-selective verification of rainfall accumulations from high-resolution forecasts of convective events. *Monthly Weather Review*, 136(1), 78–97. <https://doi.org/10.1175/2007MWR2123.1>
- Satoh, M., Stevens, B., Judt, F., Khairoutdinov, M., Lin, S. J., Putman, W. M., & Düben, P. (2019). Global cloud-resolving models. *Current Climate Change Reports*, 5(3), 172–184. <https://doi.org/10.1007/s40641-019-00131-0>
- Sela, J. G. (2010). The derivation of the sigma pressure hybrid coordinate Semi-Lagrangian model equations for the GFS.
- Snook, N., Kong, F., Brewster, K. A., Xue, M., Thomas, K. W., Supinie, T. A., et al. (2019). Evaluation of convection-permitting precipitation forecast products using WRF, NMMB, and FV3 for the 2016–17 NOAA hydrometeorology testbed flash flood and intense rainfall experiments. *Weather and Forecasting*, 34(3), 781–804. <https://doi.org/10.1175/WAF-D-18-0155.1>
- Sobash, R. A., Kain, J. S., Bright, D. R., Dean, A. R., Coniglio, M. C., & Weiss, S. J. (2011). Probabilistic forecast guidance for severe thunderstorms based on the identification of extreme phenomena in convection-allowing model forecasts. *Weather and Forecasting*, 26(5), 714–728. <https://doi.org/10.1175/WAF-D-10-05046.1>
- Sobash, R. A., Romine, G. S., Schwartz, C. S., Gagne, D. J., & Weisman, M. L. (2016). Explicit forecasts of low-level rotation from convection-allowing models for next-day tornado prediction. *Weather and Forecasting*, 31(5), 1591–1614. <https://doi.org/10.1175/WAF-D-16-0073.1>
- Sobash, R. A., Schwartz, C. S., Romine, G. S., & Weisman, M. L. (2019). Next-day prediction of tornadoes using convection-allowing models with 1-km horizontal grid spacing. *Weather and Forecasting*, 34(4), 1117–1135. <https://doi.org/10.1175/WAF-D-19-0044.1>
- Thiébaux, J., Rogers, E., Wang, W., & Katz, B. (2003). A new high-resolution blended real-time global sea surface temperature analysis. *Bulletin of the American Meteorological Society*, 84(5), 645–656. <https://doi.org/10.1175/BAMS-84-5-645>
- Van Leer, B. (1974). Towards the ultimate conservative difference scheme. II. Monotonicity and conservation combined in a second-order scheme. *Journal of Computational Physics*, 14(4), 361–370.
- Vecchi, G. A., Murakami, H., Delworth, T. L., Underwood, S., Wittenberg, A. T., Zeng, F. J., & Kapnick, S. B. (2019). Tropical cyclone sensitivity to global forcing: Seeds and probability. AGUFM, 2019, A32F-A06F.
- Vitart, F., Ardilouze, C., Bonet, A., Brookshaw, A., Chen, M., Codorean, C., et al. (2017). The subseasonal to seasonal (S2S) prediction project database. *Bulletin of the American Meteorological Society*, 98(1), 163–173. <https://doi.org/10.1175/BAMS-D-16-0017.1>
- Wei, H., Zheng, W., Meng, J., Gayno, G., Hou, Y., & Ek, M. (2017). Planned land surface changes for the next NEMS implementation. In 28th Conf. on Weather Analysis and Forecasting/24th Conf. on Numerical Weather Prediction, American Meteorological Society, Seattle, WA, pp. 600.
- Wheeler, M. C., & Hendon, H. H. (2004). An all-season real-time multivariate MJO index: Development of an index for monitoring and prediction. *Monthly Weather Review*, 132(8), 1917–1932. [https://doi.org/10.1175/1520-0493\(2004\)132<1917:AARMMI>2.0.CO;2](https://doi.org/10.1175/1520-0493(2004)132<1917:AARMMI>2.0.CO;2)
- Wilson, T. H., & Fovell, R. G. (2018). Modeling the evolution and life cycle of radiative cold pools and fog. *Weather and Forecasting*, 33, 2031–2220.
- Xiang, B., Zhao, M., Jiang, X., Lin, S. J., Li, T., Fu, X., & Vecchi, G. (2015). The 3–4-week MJO prediction skill in a GFDL coupled model. *Journal of Climate*, 28(13), 5351–5364. <https://doi.org/10.1175/JCLI-D-15-0102.1>
- Xu, K.-M., & Randall, D. A. (1996). A semiempirical cloudiness parameterization for use in climate models. *Journal of the Atmospheric Sciences*, 53(21), 3084–3102. [https://doi.org/10.1175/1520-0469\(1996\)053<3084:ASCPFU>2.0.CO;2](https://doi.org/10.1175/1520-0469(1996)053<3084:ASCPFU>2.0.CO;2)
- Yoneyama, K., Zhang, C., & Long, C. N. (2013). Tracking pulses of the Madden-Julian Oscillation. *Bulletin of the American Meteorological Society*, 94(12), 1871–1891. <https://doi.org/10.1175/BAMS-D-12-00157.1>
- Zhang, C., Xue, M., Supinie, T. A., Kong, F., Snook, N., Thomas, K. W., et al. (2019). How well does an FV3-based model predict precipitation at a convection-allowing resolution? Results from CAPS forecasts for the 2018 NOAA hazardous weather test bed with different physics combinations. *Geophysical Research Letters*, 46, 3523–3531. <https://doi.org/10.1029/2018GL081702>
- Zhang, J. A., Nolan, D. S., Rogers, R. F., & Tallapragada, V. (2015). Evaluating the impact of improvements in the boundary layer parameterization on hurricane intensity and structure forecasts in HWRF. *Monthly Weather Review*, 143(8), 3136–3155. <https://doi.org/10.1175/MWR-D-14-00339.1>
- Zhao, M., Golaz, J.-C., Held, I. M., Guo, H., Balaji, V., Benson, R., et al. (2018). The GFDL global atmosphere and land model AM4.0/LM4.0: 1. Simulation characteristics with prescribed SSTs. *Journal of Advances in Modeling Earth Systems*, 10, 691–734. <https://doi.org/10.1002/2017MS001208>

- Zhao, M., Held, I. M., Lin, S. J., & Vecchi, G. A. (2009). Simulations of global hurricane climatology, interannual variability, and response to global warming using a 50-km resolution GCM. *Journal of Climate*, *22*(24), 6653–6678. <https://doi.org/10.1175/2009JCLI3049.1>
- Zhao, Q., & Carr, F. H. (1997). A prognostic cloud scheme for operational NWP models. *Monthly Weather Review*, *125*(8), 1931–1953. [https://doi.org/10.1175/1520-0493\(1997\)125<1931:APCSFO>2.0.CO;2](https://doi.org/10.1175/1520-0493(1997)125<1931:APCSFO>2.0.CO;2)
- Zhou, L., Lin, S.-J., Chen, J.-H., Harris, L. M., Chen, X., & Rees, S. L. (2019). Toward convective-scale prediction within the next generation global prediction system. *Bulletin of the American Meteorological Society*, *100*(7), 1225–1243. <https://doi.org/10.1175/BAMS-D-17-0246.1>